
Princeton University

Department of Mathematics

Senior Thesis

# Probabilistic models for spike trains of single neurons

Author:

Marius Pachitariu

Supervisors:

Prof Carlos D Brody

PhD Joseph K Jun

Prof Philip J Holmes

**Abstract**

The primary mode of information transmission in neural networks is unknown: is it a rate code or a timing code? Assuming that presynaptic spike trains are stochastic and a rate code is used, probabilistic models of spiking can reveal properties of the neural computation performed at the level of single neurons. Here we show that depending on the probabilistic model of choice, spike trains can be more or less efficient in propagating the rate code. A time rescaled renewal process (TRRP) of relatively narrow distribution of interspike intervals can be several times more efficient than the Poisson model. However, a multiplicative Independent Markov Intervals (mIMI) model of however narrow distribution of interspike intervals appears to be only as efficient as a Poisson model. We observed fairly regular spike trains in a rat premotor area – the frontal orienting fields (FOF) – in-vivo, and we tried to determine which model – the TRRP or the mIMI – describes them better. In doing the comparison we relied on the fact that the two models make different predictions about the distributions of interspike intervals at different firing rates. Given the kind of tasks the rats are doing we were unable to directly compute these distributions, but we were able to indirectly estimate the shape parameters of the best fit gamma distributions: a special class of TRRP models. The shape parameters remained approximately constant over a wide range of firing rates (10-40 Hz) for 65% of the neurons in FOF, consistent with the TRRP model. 25% of neurons had shape parameters that increased with firing rate, consistent with the mIMI model. The remaining 9% had shape parameters that decreased with firing rate, consistent with neither of the models.

# Contents

# Part I

# Rate code is more efficient for time-rescaled renewal processes

## 1 Introduction

Neurons are thought to convey signals mainly if not exclusively through the information content of their spike trains. A spike train consists of the series of times at which the neuron has fired. It is possible to record spike trains from individual neurons using various electrophysiological methods in vivo and in vitro and such methods have generated a good number of datasets, which in turn have revealed many properties of the neural computation. Such properties constitute the main body of results in the rapidly growing neuroscience literature.

We have the opportunity to analyze two such datasets. One has been recorded in the Romo lab about ten years ago from macaques performing a delayed comparison task. The main results are described elsewhere (Romo et al. (1999), Brody et al. (2003)). The other dataset is the result of an ongoing effort of the Brody lab, where neural activity has been recorded in rats performing a variety of tasks.

For this project we are mainly interested in the statistics of the spike trains and what these statistics might tell us about the computational properties of the cells. The most widely used statistic is the so called peri-stimulus time histogram or PSTH[1]. PSTHs of individual neurons are obtained by binning individual trials, averaging the bins over all trials and then convolving with a smoothing function such as a Gaussian kernel. As a final product of this algorithm, the PSTH reveals little information about the specific timings of single spikes - most (but not all) of that information has been lost in the process. Here we will describe and use statistics of spike trains beyond the PSTH.

One fundamental aspect of spike trains recorded in vivo is that they appear to be inherently stochastic (Dayan & Abbott (2001)). The spike trains seem to be as random as possible because it is impossible to predict when the next spike will occur. Spikes are not fired at fixed intervals, instead the distribution of the intervals between spikes seems to be almost exponential. The exponential distribution has maximum entropy among all distributions with a fixed mean and support $[0, \infty)$ (Taneja (2001)). This suggests that spike trains with exponential ISI distributions are as general as they can possibly be.

This work was motivated by the following four central questions.

[1] Alternatively, if neural data is not aligned to the stimulus but to behavior or some other event, this statistic is called the peri-event time histogram, or the PETH

- **Question 1.** What kinds of statistics can we get from spike trains? What features of these statistics could be interesting?
- **Question 2.** How do we obtain these statistics from data?
- **Question 3.** Once we have the statistics of interest, can we think of mechanisms, cellular or network-level, that could explain these statistics?
- **Question 4.** Do these statistics matter? Are they important in any way to the function of neurons and networks or are the statistics just noise, a mere by-product of the cellular and network-level processes that trigger spikes?

While we believe questions 1 to 3 to be important, we think question 4 is the most intriguing one and maybe the sole reason why we should seek answers to questions 1 to 3 in the first place. An easy exercise is to answer questions 1 to 4 in the case of the PSTH.

- **Answer 1:** The PSTH. Different firing rates in different behavioral states could be interesting.
- **Answer 2:** Already described above.
- **Answer 3:** Neurons integrate excitatory post-synaptic potentials (EPSPs) to generate action potentials or spikes which they communicate across their synapses to other neurons. It is thought that the average rate of arrivals of these spikes transmits all information relevant to neural processing in perhaps most neural networks. This mode of information transmission is usually called a rate code. The PSTH describes the rate of firing of a neuron.
- **Answer 4:** If the rate code is assumed, differences in spike counts are the only thing that matters in conveying information. Significant changes in the PSTH correlated with behavior can reveal the relationship between neural signals and behavior.

Most of our work is concerned with answering questions 1 to 3 for different statistics than the PSTH. However, we attempt to give an answer to question 4 in the first part of this work before approaching the other questions. We conclude this introduction with an outline of the entire paper below.

In the first of two parts we make certain assumptions about the firing statistics of ideal model neurons and we analyze the properties of these neurons analytically and in computational simulations. More specifically, we analyze the Poisson process model, introduced in section 2.2, the time rescaled renewal process model (TRRP, Koyama & Kass (2008)), introduced in section 3 and the multiplicative independent Markov intervals model (mIMI, Kass & Ventura (2001), introduced in section 4.5. We seek to determine which of the model

neurons are efficient encoders of information. To this end we formulate a paradigm in which rate code neurons are thought to encode a predefined signal which we seek to decode in the best possible manner 4. We found that while the Poisson and the mIMI models have an SS of 1 (precise for Poisson but to a first approximation for mIMI), the TRRP model has an SS that depends on the narrowness of the interspike interval (ISI) distribution 4.4. If the coefficient of variation (**CV**) of the ISI distribution (the ratio between the standard deviation and the mean) is smaller than 1, then the SS of the TRRP model is larger than 1. This does not apply, however, for mIMI models, which can also have a relatively narrow distribution of ISIs. We interpret these results and discuss their implications in section 8.

In the second half of the paper we test whether the assumptions made about the model neurons are supported by electrophysiological data from neurons in two datasets. We were not able to directly obtain accurate distributions of ISIs from spiking data, because real neurons do not behave as stationary point processes. Instead, their intensity changes in time. We developed an indirect method to obtain an estimate of the **CV**of the ISI distributions based on the gamma distributions. Specifically, we make two assumptions. The first assumption is that the firing rates of real neurons vary on relatively long timescales compared to the mean ISI (¿2 ISIs). The second assumption is that the ISI distributions are relatively well modeled by gamma distributions. From these two assumptions we are able to determine the shape parameter of the model gamma distributions from actual spiking data. The method is described in section 5. Another important step in our analysis is to differentially analyze **CV**(or equivalently the gamma shape **K**) at different firing rates. Only then can we distinguish between the mIMI and TRRP models. To this purpose we obtain a local estimate of the firing rate by locally convolving the spike trains with gaussian or gaussian-like kernels (section 7.5). Finally we obtain a separate **K**value for each neuron in each of six firing rate ranges (from 10-15 Hz to 35-40 Hz). We compare these values with those prescribed by the three models analyzed in the first part of the paper and determine that the TRRP model fits the largest percentage (65%) of the units (section 7.6).

In the immediately following section we provide several definitions in order to fix our working concepts. We define spike trains mathematically as point processes and describe the Poisson and Gamma models. We then introduce a variety of regularity measures normally used to describe neural spike trains.

# 2 Theoretical framework

## 2.1 Elements of probability theory

Here we describe spike trains and their properties rigorously by appropriate mathematical representations. We define a **spike train** as an element $S$ of $\mathcal{R} = \bigcup_{N=0}^{\infty} \mathbb{R}^N$ with $S =$

$\{t_1 < t_2 < ... < t_N\}$ [2]. A point process is defined to be a random variable with values in the set of elementary outcomes $\mathcal{R}$. We restrict our attention to subsets of $\mathcal{R}$ of the form $\mathcal{R}[T_1, T_2] = \{S \in \mathcal{R} | S = \{t_1, t_2, ..., t_N\}$ and $T_1 \leq t_k < T_2, \forall k\}$. $\mathcal{R}[T_1, T_2]$ is the space of point process starting at $T_1$ and ending at $T_2$. In practice $T_1$ and $T_2$ should be taken to be the beginning and ending time of each recorded trial, because we are interested in the multiple realizations of presumably the same point process over different trials. Spike trains from all trials can be considered realizations of independent identically distributed (iid) variables.

For each spike train $S$ we define an associated series of interspike intervals (ISIs) $I_S = \{t_1 - T_1, t_2 - t_1, t_3 - t_2, ..., t_N - t_{N-1}\}$. $I_S$ is also the realization of a random variable and in certain cases it will be more convenient to consider $I_S$ rather than $S$.

We turn our attention to a very popular model for spike trains, the homogeneous Poisson process, for which we can easily define a number of characteristic statistical properties. The Poisson model has been adopted as the null hypothesis by much of the neuroscience community, given its general adequacy in describing spike data recorded in vivo. The properties which account for its success are:

- independence of ISI intervals. If we write $I_S = \{\text{ISI}_1, \text{ISI}_2, ..., \text{ISI}_{N-1}\}$ then we can consider $\text{ISI}_k$ as the realization of a random variable $\mu_k$. The independence property is then equivalent to $\mu_k$ and $\mu_{k'}$ being independent for all $k \neq k'$. [3]

- $\mu_k \sim \mu$ for all $k$. The ISIs are independent draws of identically distributed random variables. From here on we relinquish this formality by saying that the ISIs are independent draws of the same random variable $\mu$.

- $p_\mu(x) = \lambda e^{-\lambda x}$ or $\mu$ has exponential distribution. $\dfrac{1}{\lambda}$ is the mean ISI and $\lambda$ is the intensity of the process. For spike trains we also call $\lambda$ the mean firing rate.

In our analysis we always assume the first property but never the following two. The second property specifies a stationary point process but spike trains recorded in cortex most often show strong variations in firing rate, especially in relation to behavioral events. We suggest other probability distributions to replace the exponential. Gamma distributions are the most natural and popular choices (Seal et al. (1983), Maimon & Assad (2009)). These distributions are specified by probability densities of the form

$$f(x; k, \theta) = x^{k-1} \frac{e^{-x/\theta}}{\theta^k \Gamma(k)}, \tag{2.1}$$

[2] We loosely follow the notation and definitions of Sahani (2007)

[3] Notice we depart here from Sahani (2007) in that we consider the Poisson process in terms of its associated ISI random variables and not its associated counting process. The reason is that the counting process is ultimately useful for describing PSTHs and we want to keep more information about spike timings *relative to each other*.

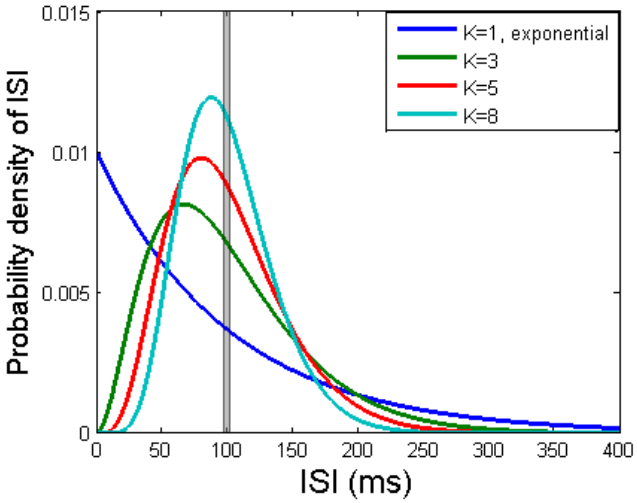


Figure 1: Probability densities of random variables with gamma distribution. All distributions shown have the same mean $k\theta = 100$ but different shape parameters $k = 1, 3, 5, 8$. The scale parameter $\theta$ has been chosen such that $k\theta = 100$. $k = 1$ represents a purely exponential distribution, for which the polynomial part $x^{k-1}$ in the defining equation (2.1) is constant 1.

where the gamma function is given by $\Gamma(z) = \int_0^\infty t^{z-1}e^{-t}\,dt$. Figure 1 shows a few examples of gamma distributions with the same mean $(k\theta)$ but different shape values, $k$. For $k = 1$ the distribution is exponential, the ISI distribution of a Poisson random process, but for increasing $k$ the distribution becomes more and more narrow around the mean.

### 2.2 Classical regularity measures for spike trains

In this section we review a number of methods to describe the regularity of a spike train. Intuitively, the measures we give below quantify how regularly spikes are spaced out together.

1. The coefficient of variation **CV** is given by $\mathrm{CV} = \dfrac{\sqrt{\mathrm{Var}(\mu)}}{\mathrm{E}(\mu)}$, where $\mu$ is the random variable underlying the ISI instantiations and $\mathrm{Var}(\mu) = \mathrm{E}(\mu - \mathrm{E}(\mu))^2$. For a Poisson process $\mathbf{CV} = 1$. For gamma distributions $\mathbf{CV} = \dfrac{1}{k}$ (Shinomoto et al. (2003)).

2. **K** is the shape parameter of the best fit gamma distribution to $\mu$. A high shape parameter **k** will underlie a regular process.

   *Note.* The intensity of a random process is always given by $\dfrac{1}{\mathrm{E}(\mu)}$ (Sahani (2007)). For spike trains this corresponds to the firing rate. A process is called stationary if it maintains a constant intensity in time. The measures we have just defined assume that the underlying process is stationary, but spike trains are most usually non-stationary. The following two measures were designed to overcome the problem of non-stationarity.

3. $\mathbf{CV_2}$ is obtained from a sequence of ISIs by first computing the associated sequence

$$CV_2(n) = \frac{2|\mathrm{ISI}_n - \mathrm{ISI}_{n+1}|}{\mathrm{ISI}_n + \mathrm{ISI}_{n+1}}$$

and then taking the average over $n$, $\mathbf{CV_2} = \langle CV_2 \rangle$ (Holt et al. (1996) Compte et al. (2003)). $\mathbf{CV_2}$ is approximately equal to $\mathbf{CV}$ for gamma processes over a wide range of parameters $k$ and $\theta$, but $\mathbf{CV_2}$ is also independent of variations of intensity on time scales longer than two ISIs. Therefore $\mathbf{CV_2}$ is more accurate estimate of the regularity of a slowly varying non-stationary process than $\mathbf{CV}$.

4. $\mathbf{k}_{x-y\text{Hz}}$ is the shape parameter of the best fit gamma distribution to the histogram of ISIs drawn from a random process with intensity between $x$ and $y$ Hz (Maimon & Assad (2009), Softky & Koch (1993)). If the range $(x, y)$ of intensities is small enough, for example 5 Hz, the error in estimating the shape parameter from the ISI histograms will be small. The main difficulty with this method is that one needs to estimate the intensity of the process from other sources than the ISI itself, for example by calculating the expected firing rate from the PSTH of multiple similar trials (Maimon & Assad (2009)).

   *Note.* We will use a combination of the previous two methods. Unlike Maimon & Assad (2009) we estimate the firing rate from a different source than the PSTH but from there we continue with parsing histograms by firing rate. Instead of fitting the resulting ISI histograms with gamma distributions we will instead estimate the shape parameter from a statistic similar to $\mathbf{CV_2}$.

5. The Fano Factors are given by $\mathbf{F}(T) = \dfrac{\sigma(T)^2}{P}$ where $P = \text{Mean}(T)$ is the mean number of occurrences in some window of time length $T$ and $\sigma(T)^2$ is the variance of the process in that window, over multiple trials. For a Poisson process $\mathbf{F}(T) = 1, \forall T > 0$.

   *Note.* The Fano Factors are a measure not only of the regularity of the process but also of the reproducibility of the process across multiple trials. If there are strong covariations between stimulus and firing rate, then the spike train might in principle be more reproducible from trial to trial than a random process will predict. Conversely one should expect larger Fano Factors if there is additional noise in the intensity of the random process across trials.

   *Note2.* It is important to consider that the Fano Factor is a function of $T$ for non-Poisson processes. For example, as $T \to 0$, $\mathbf{F}(T) \to 1$ and the process becomes nearly binomial in short windows (Ratnam & Nelson (2000)). Also, as $T \to \infty$, $\mathbf{F}(T) \to \mathbf{CV}^2$ (Cox (1967), Nawrot et al. (2008)). Another property of the Fano Factor is that is bounded from below by $\dfrac{p(1-p)}{P}$ where $P = \text{Mean}(T)$ is the mean of the process and $p$ is the fractional part of $P$ (vanSteveninck et al. (1997)). For our purposes we will need to know how fast the approximation $\mathbf{F}(T) = \mathbf{CV}^2$ becomes reliable; we will consider the issue later in section 3.2.

We also designed another measure of regularity **K**. **K** approximates the shape parameter of the best fit **non-stationary gamma process**. A **non-stationary gamma process** is defined to be a random process generated by drawing ISIs from gamma distributions of a fixed shape parameter $k$, but of possibly varying scale parameters $\theta$. There are a number of reasons why it is advantageous to use **K** as a regularity measure for most of the analysis and we describe **K** in section 5 in the second part of our paper (for two related measures obtained in similar ways, $Lv$ and $LvR$, see Shinomoto et al. (2003) and Shinomoto et al. (2009)).

We begin in the next section to describe a special class of probabilistic models for neurons.

# 3 The ideal time-rescaled model neuron

The first description of a time-rescaled model neuron that we know of belongs to Reich et al. (1998). They call it 'simply modulated renewal process' (SMRP). Another mention of such renewal processes is made in Koyama & Kass (2008), where the authors call the model a time-rescaled renewal process (TRRP). We prefer the second nomenclature, mainly because of the desirable association with the time-rescaling theorem (Brown et al. (2001)).

We call a model neuron or a renewal process time-rescaled if the distribution of its interspike intervals satisfies

$$\text{Prob}(\text{ISI} < x|R) = \text{F}(xR), \tag{3.1}$$

where $R$ is the firing rate and F is some cumulative distribution function with support $[0, \infty)$. Notice this does not specify what the distribution of ISIs should be at a given firing rate, but it specifies how the distribution should scale with firing rate. For example, subfamilies of gamma distributions satisfy this criterion. These subfamilies have the form $f\left(x; k, \frac{1}{Rk}\right)$ for fixed $k$ and varying firing rates $R$. To see that these families satisfy (3.1), let us first transform (3.1) in its probability density version. We denote the probability density of the ISI distribution by $p(x, R)$.

$$\begin{aligned} p(x,R)\,dx &= \text{Prob}(x < \text{ISI} < x + dx|R) \\ &= \text{F}((x+dx)R) - \text{F}(xR) \\ &= \text{F}'(xR)R\,dx. \end{aligned} \tag{3.2}$$

For the gamma distributions we have

$$
\begin{aligned}
p_{\text{gamma}}(x, R)\, dx &= f\left(x; k, \frac{1}{Rk}\right) \\
&= x^{k-1} \frac{e^{-xRk}}{\left(\frac{1}{Rk}\right)^k \Gamma(k)} \\
&= g(xR) R\, dx.
\end{aligned}
$$

where $g(y) = \dfrac{k^k}{\Gamma(k)} y^{k-1} e^{-yk}$. If we identify $g$ with $\mathrm{F}'$ we obtain that the gamma family satisfies (3.2) from which it follows that it satisfies (3.1). One special gamma family is that of the exponential distributions, for which $k = 1$ and which results from Poisson processes.

### 3.1 Evidence for TRRPs in datasets

It has been shown that the ISI histograms of neurons in visual motion areas of macaques (MT/MST, LIP and Area 5) are well fitted by gamma distributions (Maimon & Assad (2009)). These neurons fire at a variety of rates but the authors of this study showed that for a given neuron, the shape parameters $k$ of the best fits with gamma distributions remain almost constant while only the scale parameter $\theta$ varies (Maimon & Assad (2009)). To show this, they parsed the collection of ISIs into subsets associated with similar firing rates. In total they had 6 different ranges of firing rates from $10 - 15$ Hz to $35 - 40$ Hz. They separately fit one gamma distribution to each set of ISIs. The same method had been used before by Softky & Koch (1993) to analyze neurons in primary visual cortex (V1) and MT.

The fact that the shape parameter is the same at different firing rates in these three visual areas is an important result because it is the first evidence of neurons in vivo that act as regular TRRPs that we know of. In contrast, Reich et al. (1998) which first mentioned the 'simply modulated renewal process', defined it simply to show that it does not fit ISI distributions better than other models with fixed refractory periods in cat retinal ganglions, cat lateral geniculate nucleus (LGN) and in macaque V1 (Reich et al. (1998)). Koyama & Kass (2008) showed that the TRRP fits leaky integrate and fire neurons well if the mean of the input stays the same while the variance changes. However, unlike Maimon & Assad (2009) they do not provide an estimate of the regularity of the simulated neurons. The gamma distributions fitted by Maimon & Assad (2009) had high average shape parameters of 2.7 in Area 5, 1.95 in LIP and only 1.23 in MT/MST. Several neurons were fitted with shape parameters larger than 10.

The reason we should care deeply about regularity is hinted at by a number of authors (Maimon & Assad (2009), Prescott & Sejnowski (2008)). They correctly specify that highly regular processes result in low Fano Factors and therefore low variability of spike counts across trials. It seems intuitive then that regular processes will result in a sharpening of

the rate code. We show in section 4.5 that increased regularity by itself need not sharpen the rate code in general, but in section 4.4 we show that regularity does sharpen the rate code for TRRP models. The counterexample of section 4.5 is a popular choice for modeling point processes, the multiplicative Independent Markov Intervals (mIMI) model (Kass & Ventura (2001), Berry & Meister (1998), Koyama & Kass (2008)). The mIMI is a model for point processes with a fixed refractory-like period. In contrast, the TRRP model scales any refractory-like period (Reich et al. (1998)).

The second in vivo dataset displaying regular neurons with the time-rescaling property that we know of is that recorded by the Brody lab. This is one of the two datasets available to us for the analysis which we perform in the second part of this work. A large proportion (65%) of the neurons recorded in a premotor area of the rat brain named Frontal Orienting Fields (FOF) followed the TRRP model over a wide range of firing rates (10-40 Hz).

We should also add here a third and a fourth candidate datasets with regular TRRP neurons, one recorded in slice but under simulated in vivo conditions (Chance & Abbott (2002)) and one recorded in the isolated retina (Levine & Shefner (1976)). Chance & Abbott (2002) stimulated neurons with excitatory and inhibitory currents at 7000Hz and 3000Hz respectively with noise of various means and variances and they recorded spikes extracellularly. The results which we are interested in are presented in figure 3E of their paper. The coefficient of variation stays approximately constant and relatively low (0.5-0.6) in a wide range of firing rates (5-50 Hz) (Chance & Abbott (2002)). The fourth candidate data set is presented in Levine & Shefner (1976) and consists of ganglion cells in goldfish retina. The authors found that the **CV** of these cells stays approximately constant and low ($\sim 0.3$) over a wide range of firing rates.

As a fifth independent line of evidence for regular TRRPs we mention a recent meta-study of 19 data sets. Shinomoto et al. (2009) found that a certain measure of regularity does not depend on firing rate in a number of distinct brain areas. The specific measure they use, which they call $LvR$, is only indirectly related to **CV** or gamma shapes, so its constancy needs not necessarily mean that **CV** is the same at all firing rates; however the approximation is still of interest. Interestingly, Shinomoto et al. (2009) found that there is a progression of regularity from visual sensory areas to motor areas, with motor areas being most regular. A similar progression has been found by Maimon & Assad (2009) from low-order visual to high-order visual areas. In particular, Area 5 was found by Maimon & Assad (2009) to have average gamma shapes of $\sim 3$ which would imply a coefficient of variation of $\frac{1}{\sqrt{3}} \sim 0.6$ : very close to the average that we found in rat FOF and very close to the averages found by Shinomoto et al. (2009) in monkey M1, SMA and SEF.

### 3.2 Fano factors for TRRPs at different firing rates are asymptotically equal

We begin the analysis of the TRRP model by considering the Fano factors. We cited a couple of results in section 2.2, the most important of which is that asymptotically

$$\mathbf{F}(T) \approx \mathbf{CV}^2, \tag{3.3}$$

regardless of the renewal process considered (Cox (1967)). Since TRRPs at different rates have their ISI distributions scaled by a factor and **CV** is just the ratio of standard deviation and mean, it follows that **CV** is the same at all firing rates and asymptotically the Fano Factors for TRRPs are the same at all firing rates. How large does $T$ have to be to get close to the approximation of (3.3)? To get a feeling for the rate of convergence we ran computational simulations of gamma processes of different shape values. The Fano Factor was close to convergence in all cases when $T > \frac{3}{Rate}$, or in other words when $T$ was about twice the length of the mean ISI. We care about processes at intensities in the range of $10 - 40$ Hz, so Fano Factors in intervals $\geq$ 200ms should be close to the asymptotic value $\mathbf{CV}^2$ for such intensities. Note that for some systems, like visual cortex, timescales of 200 ms and more are not acceptable, but in higher level processing like decision making such timescales are common place. Even so we are allowed to make the approximation (3.3) in shorter time windows for visual neurons when the firing rates are high, which is common in sensory systems. For our purposes we analyze random processes in windows of at least 200 ms but the analysis is the same for higher intensity random processes in shorter windows.

It is also true that asymptotically the distribution of spike counts is Gaussian (Cox (1967)). Again, for $T > \frac{3}{Rate}$ this approximation becomes good. We will need this result in the next section, together with the approximation from equation (3.3).

## 4 Signal per Spike (SS)

### 4.1 How do we measure rate code efficiency?

In this section we want to start describing measures of rate code efficiency. We want to directly contrast our method and view with that of Prescott & Sejnowski (2008). There the authors investigate a different model neuron than ours, however the conclusions on rate code efficiency are similar. Their two mechanistic model neurons include different forms of spike-rate adaptation, which they show to have differential effects on the coding properties of the model neurons (Prescott & Sejnowski (2008)). They argue that the model neuron, which includes an after-hyperpolarizing potassium current ($I_{AHP}$), enhances the spike-rate code by virtue of both regularizing the distribution of ISIs and by creating a strong negative correlation between consecutive ISIs. Since in our probabilistic models consecutive ISIs are

independent, we can only directly compare our model with theirs through the effect that ISI regularization has on rate coding.

To make their point they apply a 5 Hz sine wave input signal to their model neurons and calculate the signal to noise ratio (SNR) defined as the ratio between the power at 5 Hz for the response with the 5 Hz input and the power at 5 Hz for the response without the 5 Hz input but equivalent noise (Prescott & Sejnowski (2008), see figure 4D). For the model with regularized ISIs they obtain SNR = 6.8 and for the model without regularized ISIs they obtain precisely the same SNR (we believe this is no coincidence, see section 4.5 for a similar 'coincidence' between the probabilistic Poisson and mIMI models). However, they go on to argue that the second model obtains that SNR by virtue of a higher spike modulation around baseline ($25 \pm 4.4$ spikes/s as compared with $25 \pm 1$ spikes/s) and for some reason they discard this. Then they adjust the amplitude of the input sine wave to the second model so as to obtain the same $\pm$ 1 spike modulation and calculate the SNR again, obtaining only SNR = 1.3 this time. They finally compare this new SNR of 1.3 with the old SNR of 6.8 to argue that the model with $I_{AHP}$ is a better rate encoder than their other model. The crucial step in their argument, which we object to, is that higher spike modulation around baseline is not useful or should not be allowed as a variable in the comparison.

In a previous argument in the same paper (Prescott & Sejnowski (2008), see figure 4C), the authors argue that average firing rates should be equated when comparing the regularity of two model neurons. Of course, more spikes give a larger capacity for storing information in their patterns. But spikes are expensive and so neurons cannot just use as many spikes as they please to transmit information. Instead they have to balance their firing rates against the costs of generating spikes. We believe this should indeed be the guiding principle in designing efficient neurons. We also believe that Prescott & Sejnowski (2008) intended to extend this principle to the case of spike rate modulation. However, the argument which we just gave about spike costs no longer applies for spike rate modulation if the mean firing rates are the same.

Consider a neuron as a simple input to output device. Its job is to integrate continuous signals (excitatory post-synaptic potentials, EPSPs) and generate a discrete output — spikes. The spikes should carry as much information about the continuous signals as possible. It is obvious that much information will be lost in the conversion, but the biological constraints enforce such limitations: information can be communicated over much longer distances by spikes than by any chemical signal. The other important biological constraint that needs to be considered is the cost of a spike. Most of the energy spent by the brain goes into maintaining the electrochemical gradients between the inside and outside of neurons, which gradients are disturbed mostly by the generation and transmission of spikes (Kandel et al. (2000)). Therefore the right question to ask when considering the efficiency of any

code, be it a rate code or a timing code, is how much information does a spike train carry about the input as a function of the average number of spikes which that neuron uses, and to allow as much spike rate modulation as necessary. If anything, it would seem that more spike rate modulation is better, since it provides a larger range of output values.

There is another issue in the methods of Prescott & Sejnowski (2008) that we would like to address. It seems they assume that the crucial information which a neuron encodes about a stimulus is its periodicity or power spectrum, therefore any two signals with the same periodicity are equivalent input, which gives them the freedom to adjust the amplitude of the sine wave as they do while saying that they have not changed the signal. Again we think this is the wrong approach. It may certainly be the case that in some situations, in some neural systems, the periodicity of the stimulus is the quantity of interest. But we think that much more often the quantities of interest are instantaneous variations in the stimulus, where stimulus here must be understood as the input to the neuron. Is the stimulus **currently** higher or lower than expected? With this in mind we propose a different kind of signal to noise measure which we call the signal per spike measure (**SS**). We argue that the **SS** is a more intuitive and useful measure of how efficient a given neuron is as an input to output device.

### 4.2 The Two-Class Neuron

To begin describing the **SS** we need to state the signal encoding problem more concisely. As noted in the previous section, the job of a neuron after integration of its presynaptic signals is to transform the continuous subthreshold voltage trace into a sequence of action potentials. Our working model does not address the integration part at all, but instead focuses on the spike generation part. In our model the input to a neuron is just some scalar quantity which is then transformed by a function into an instantaneous probability to fire. It is important not to confuse this input with the membrane voltage. When the membrane voltage reaches the threshold a spike is initiated in a deterministic fashion. Likewise, the EPSPs are deterministic events; however, they occur at unpredictable times and are the result of a barrage of unsynchronized spikes from other neurons. The point process models the non-predictability of the membrane voltage by assuming there is an underlying constant signal or input on top of which a number of sources of noise are overlayed resulting in variable spike times.

What kinds of inputs should we consider? If the input is always the same, then there is no information for the spike train to encode. If the input is half of the time $x$ and half of the time $y \neq x$ then there is exactly one bit of information to encode. If the input is more generally continuous then the information to be encoded can be larger, and potentially infinite. It is still a matter of controversy whether neurons or networks can function as

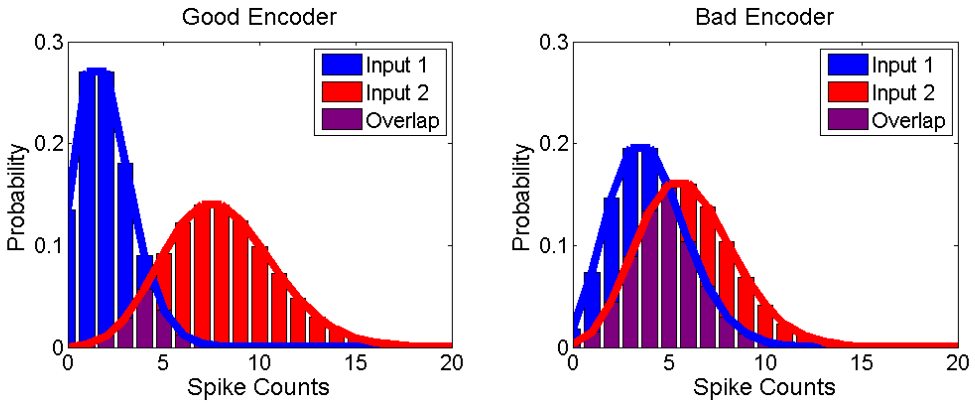


Figure 2: The good, the bad and the ugly. We illustrate the output distributions of total number of spikes in one second for two model Poisson neurons firing at a) 2 and 8 Hz b) 4 and 6 Hz. The means of both pairs of distributions are 5 but the overlap is much larger for b).

analog devices (see for example Machens et al. (2005) for a model of analog short memory storage). Therefore it is unknown if neurons act more like discrete classifiers or more like continuous ones, but there is enough noise in neural systems to blur out even discrete signals into something continuous. Regardless of what the neuron's job as a classifier is, the output in spikes should be 'close' to some target output that specifies the information downstream. A neuron encodes a rate code better when the differences between the spike counts and the target outputs is minimized. To anticipate latter developments in this section, the more efficient neuron will have the smaller squared error from the target outputs.

Consider the simple neuron whose job is to encode only two different inputs. Suppose for now that the two-class neuron follows a Poisson model and that we are counting spikes in a bin of size 1000 ms. Variant one of the two-class neuron fires at 2 Hz for input 1 and at 8 Hz for input 2. Variant two fires at 4 Hz for input 1 and 6 Hz for input 2. It is clear that these two variants fire the same average number of spikes in 1000 ms, exactly 5. It is also clear that the first variant is a good encoder, while the second one is a poor encoder, because the distributions of outputs do not overlap much in the first case (see figure 2a) but they overlap significantly in the second case (see figure 2b). The first variant is a more efficient two-class neuron because it can give more information with the same average number of spikes. It is also clear that the most efficient two-class neuron would be one that fires at 0 Hz for input 1 and 10 Hz for input 2. This example illustrates very clearly that more spike rate modulation is beneficial for the rate code.

Here is another issue we need to take into account. Consider again variant one of the two-class neuron above. When we observe 10 spikes in 1000 ms we can be sure the neuron is firing at 8 Hz, under input 2. But this belief depends crucially on the fact that we knew in advance the prior distribution of inputs. Had we known nothing about the prior distribution of inputs and we observed 10 spikes, our best estimate of the firing rate would

be 10 Hz.

### 4.3 Prior distribution and squared error

Do the classifiers downstream have knowledge about this prior distribution of inputs or not? Can the prior distribution be learned by neurons and are there appropriate neural mechanisms to perform a Bayesian inference about the input? Perhaps not for continuous signals, but the problem can be clearly solved for discrete inputs. For the two-class neuron we can imagine a threshold being implemented by a downstream neuron and having this other neuron fire a spike only when the threshold is reached. The prior distribution of the two classes of inputs will be learned by adjusting this threshold, or equivalently by adjusting the connection strength between the two-class neuron and the downstream neuron and a perfect Bayesian inference can be made with an optimal threshold. This strategy could also work for a multi-class neuron, where there are more than two distinct classes of inputs, if we consider multiple thresholds implemented by different neurons downstream. However, as soon as we introduce continuous signals the thresholding approach does not work anymore. We cannot in general answer the question posed at the beginning of this paragraph but we will assume for the rest of this work that classifiers downstream do not use information about the prior distribution of inputs. We are in the case where the best inference from observing 10 spikes in 1000 ms is 10 Hz, no matter what the range of inputs is. In future work we might approach the Bayesian question as well, though it is not immediately clear how we should proceed.

We make the following assumptions about the continuous signal which constitutes the input. First we define its distribution to be $p_I(x)$ and assume w.l.o.g. that it has a mean of 1. We do this in order to have a normalized input because later we will consider squared errors that depend on the magnitudes of the input $x$. To have a mean firing rate of 5 Hz the input $x$ should be scaled by a factor of 5 spikes/s. As a second assumption, the distribution $p_I$ should have support on $[0, \infty)$ otherwise it could become tricky to output spike counts from $\mathbb{N} = \{0, 1, 2...\}$. Let us define the random variable $\eta_x$ which takes $x$ to the final output $n \in \mathbb{N}$ – the number of spikes – and define its probability distribution

$$F(x, n) = \text{Prob}\left(\eta_x = n | x\right).$$

The function $F$ is implicitly encoded by the model neurons. Since we are not including information about $p_I$, we can obtain an optimal decoder of spike counts by maximizing the likelihood function (Kass et al. (2005), Fisher (1922)). The decoder will be optimal in the sense that it will asymptotically minimize the expected squared error between the decoded value and the actual value. Since the likelihood function is simply $L(x) = F(x, n)$, the maximum likelihood estimate (MLE) is $G(n)$ where

$$G(n) = x_0$$
$$\text{such that } F(x_0, n) = max\left[F(x, n)\right]. \tag{4.1}$$

If we include information about the prior distribution $p_I$, we would have to use a different method: the maximum a posteriori estimate (MAP) (Hastie et al. (2001)). Equation (4.1) would change to

$$G_{Bayes}(n) = x_0$$
$$\text{such that } F(x_0, n) \cdot p_I(x_0, n) = max\left[F(x, n) \cdot p_I(x, n)\right]. \tag{4.2}$$

The error is then given by $err = G(\eta_x) - x$ (or $err = G_{Bayes}(\eta_x) - x$) and the expected squared error is

$$\mathrm{E}\left(err^2\right) = \int_0^\infty \left[G(\eta_x) - x\right]^2 \, dp_I(x) \tag{4.3}$$
$$= \int_0^\infty \sum_{n=0}^{\infty} [G(n) - x]^2 \, F(x, n) \, dp_I(x). \tag{4.4}$$

To continue from here, one has to replace $G(n)$ from equation (4.1) or (4.2) into (4.4) but the expression would become so complicated that we could not hope to solve or understand it, except for the most simple of functions $F$. Instead, we try to determine $F$ and the properties of $G$ for model neurons.

We can now define the signal per spike (**SS**) measure of encoding efficiency. It will be

$$\mathbf{SS} = \frac{1}{\mathrm{E}\left(err^2\right) \cdot \langle N \rangle}, \tag{4.5}$$

where $\langle N \rangle = \int_0^\infty \mathrm{E}(\eta_x) \, dp_I(x)$ is the expected number of spikes. Notice this is the ratio between the Fisher information (inverse of minimal squared error) and the number of spikes (Kass et al. (2005), Fisher (1922)). The reason this definition is meaningful will become clear once we start calculating some **SS**'s in later sections.

## 4.4 Encoding and decoding spike counts for Poisson and TRRP

We need to connect the function $F$ defined above to some explicit models of spike generation and obtain the **SS**'s. We focus in this subsection on the Poisson and TRRP models and in the next subsection on the mIMI model.

Even though the Poisson model is in fact a special case of a TRRP, we will first derive **SS** for the Poisson in separation, because it helps illustrate the method more clearly. For

an intensity $\lambda$ in a time window of $T$ seconds the Poisson neuron produces spike counts distributed as $\eta = Pois(\lambda T)$, such that

$$\text{Prob}(\eta = n) = \frac{(\lambda T)^n \, e^{-\lambda T}}{n!} \tag{4.6}$$

and the maximum likelihood estimate of the intensity is the observed spike count $n$ divided by $T$, as one can see by differentiating equation (4.6) with respect to $\lambda$. To connect the continuous variable $x$ with the intensity we just multiply $x$ by a constant $\lambda = x \cdot c$. The resulting $F$ function can be specified as

$$F(x, :) \sim Pois(x \cdot c \cdot T). \tag{4.7}$$

The maximum likelihood estimate of $x$ is just $G(n) = n/(cT)$, where $n$ is the spike count. We can substitute this in equation (4.4) to get

$$\begin{aligned}
\text{E}(err^2) &= \int_0^\infty \sum_{n=0}^{\infty} [G(n) - x]^2 \, F(x, n) \, dp_I(x) \\
&= \int_0^\infty \sum_{n=0}^{\infty} \Big( \frac{n}{cT} - x \Big)^2 \, \frac{(xcT)^n e^{-xcT}}{n!} \, dp_I(x) \\
&= \frac{1}{T^2 c^2} \int_0^\infty \sum_{n=0}^{\infty} (n - xcT)^2 \, \frac{(xcT)^n e^{-xcT}}{n!} \, dp_I(x) \\
&= \frac{1}{T^2 c^2} \int_0^\infty \text{Var}\left(Pois(xcT)\right) dp_I(x) \\
&= \frac{1}{T^2 c^2} \int_0^\infty xcT \, dp_I(x) \\
&= \frac{1}{Tc}.
\end{aligned} \tag{4.8}$$

In the derivation above we used the fact that the variance of a Poisson random variable is equal to its mean – $\text{Var}\left(Pois(xcT)\right) = xcT$. We also used the fact that the distribution of $x$ has mean 1 by assumption. The distribution of $Pois(xcT)$ has mean $xcT$ and the average expected number of spikes is therefore $cT$. We can now plug these values into equation (4.5) to get that $\mathbf{SS} = 1$ for a Poisson random variable. It depends neither on $c$ nor on the distribution of $x$. The amount of Fisher information per spike is 1 and the accuracy (squared error) of a Poisson encoder/decoder is exactly $\frac{1}{\langle N \rangle}$, where $\langle N \rangle$ is the expected number of spikes.

Consider again the model Poisson neuron in figure 2a. If we include the priors, Bayesian decoding can almost perfectly distinguish between the two inputs. If we were to neglect information about the priors, then the average squared error would be the same as that for the encoder in figure 2b, as evidenced by the calculation we just did. This might seem to undermine our claim in section 4.2 that more spike rate modulation is advantageous

to a rate code but in fact it only points to an implicit assumption that we made. The distribution of inputs $p_I(x)$ has to be fixed before we start asking which neuron encodes $x$ more efficiently. It will be seen in section 4.5 that a different model neuron is less efficient for a fixed distribution of $x$ because it has less spike rate modulation. This paragraph raises another question as well. Do we get to choose what $x$ is? No, the brain does. $x$ represents some feature of the stimulus that has already been partly processed. Our analysis starts with a fixed distribution of $x$, whatever that might be. However, the **SS** turns out not to depend on this fixed input distribution, as we have already seen in the case of the Poisson model and as we will see for the other models as well.

For TRRP models we scale $x$ to $\lambda = xc$. We consider TRRPs in time windows $T$ long enough that the approximation $\mathbf{F}(T) \approx \mathbf{CV}^2$ holds (equation (3.3)). Another asymptotic result like (3.3) is that the distribution $D(\lambda, n) = \text{Prob}(\lambda = n)$ of spike counts $n$ or occurrences is approximately Gaussian (Cox (1967)) with mean $\lambda T$ and variance $\lambda\, T\, \mathbf{F}(T) \approx \lambda\, T\, \mathbf{CV}^2$ (see section 3.2). We can use this to show that for large enough $T$ the maximum likelihood estimate of $\lambda$ is the number of spikes divided by $T$ $\left(G(n) = \dfrac{n}{T}\right)$ by differentiating $D$ with respect to $\lambda$ like before. We omit the details of the derivation here and proceed to calculate the expected squared error from equation (4.4)

$$\begin{aligned}
\mathrm{E}(err^2) &= \int_0^\infty \sum_{n=0}^{\infty} [G(n) - x]^2 \, F(x,n)\, dp_I(x) \\
&= \frac{1}{T^2 c^2} \int_0^\infty \sum_{n=0}^{\infty} (n - xcT)^2 \, F(x,n) dp_I(x) \\
&= \frac{1}{T^2 c^2} \int_0^\infty \mathrm{Var}(\eta_x) dp_I(x) \\
&= \frac{1}{T^2 c^2} \int_0^\infty \mathbf{F}(T) \mathrm{E}(\eta_x) dp_I(x) \\
&\approx \frac{1}{T^2 c^2} \int_0^\infty \mathbf{CV}^2 xcT dp_I(x) \\
&= \frac{\mathbf{CV}^2}{Tc}.
\end{aligned} \tag{4.9}$$

We have used above the property that $\mathrm{E}(\eta_x) = xcT$ for rescaled processes, as shown in Koyama & Kass (2008). Since the mean spiking rate is $cT$, we have from equation (4.5) that $\mathbf{SS} = \dfrac{1}{\mathbf{CV}^2}$ for TRRPs, independent of $c$ and of the distribution of $x$. In particular, for gamma time-rescaled processes we have $\mathbf{SS} = k$. Notice this derivation depended crucially on the fact that **CV** is the same at all firing rates. For other models, like the mIMI which we describe in the next section, this property does not hold and the derivation of the **SS** is not completely tractable. Instead, we will approximate.

How good is $\mathbf{SS} = k$ for $k > 1$ compared to $\mathbf{SS} = 1$ for $k = 1$? An equivalent way maybe of asking the question is how many Poisson neurons with the same input $x$ does it

take to make the error as small as that obtained by a neuron with **SS** $= k$. Suppose we have $n$ Poisson neurons with a common input. Our best estimate of the common intensity is the average of the spike counts. The variance of this average is $\frac{1}{n}$th of the variance for one neuron, so the new Fano factor is divided by $n$. Mimicking the calculation in (4.8) for the average of $n$ Poisson neurons we see that the squared error is the error of a single Poisson neuron divided by $n$. Since the squared error for the gamma TRRP is proportional to $\frac{1}{k}$, it follows that a single gamma TRRP of shape parameter $k$ does as well as $k$ Poisson neurons, but the latter use $k$ times more spikes, so the energy requirement is also $k$ times more. The mean $k$ values for neurons in Area 5 of macaque brain and FOF of rat brain are about 3 so it follows that on average neurons in these areas count as 3 Poisson neurons in a rate code (but remember the no-priors assumption — the differences might be smaller if priors are used).

### 4.5 Multiplicative Independent Markov Intervals (mIMI)

We follow here the original description of the mIMI model in Kass & Ventura (2001) but a similar model was used earlier by Berry & Meister (1998). The model defines the intensity of a renewal process at time $t$ by

$$\lambda(t) = \lambda_1(t) \cdot \lambda_2(t - s_*(t)), \tag{4.10}$$

where $s_*(t)$ is the time of the last spike at time $t$. Notice that the Poisson process is a special case of the mIMI model when $\lambda_2 = 1$ is constant. [4] Like before, we assume an input $x \geq 0$ with the mean of the distribution of inputs 1 and we use a linear function to take $x$ into $\lambda_1 = cx$. We abolish the time-dependency of $\lambda_1$ because we are modeling approximately stationary processes in relatively short time windows ($T = 200 - 500$ ms). $\lambda_2$ is similar to the recovery function previously defined for TRRP models.

The distribution $p$ of ISIs can be derived directly from equation (4.10).

$$\begin{aligned} p(x)dx &= \text{Prob}(x < ISI < x + dx) \\ &= \text{Prob}(x < ISI < x + dx | x < ISI)\, \text{Prob}(x < ISI) \\ &= \lambda_1\lambda_2(x)dx \left(1 - \int_0^x p(t)\, dt\right) \\ &= \lambda_1\lambda_2(x)dx \exp\left(-\int_0^x \lambda_1\lambda_2(y)\, dy\right). \end{aligned} \tag{4.11}$$

We have used the result that $\text{Prob}(ISI < x) = \exp(-\lambda_1\lambda_2(x))$ which can be easily proved by discretizing $[0, x]$ into small bins and letting the size of the bins go to 0. It is clear from (4.11) that we can also obtain $\lambda_1\lambda_2(x)$ from the ISI distribution $p(x)dx$ by

[4] Kass & Ventura (2001) show how to fit such a model to spiking data.

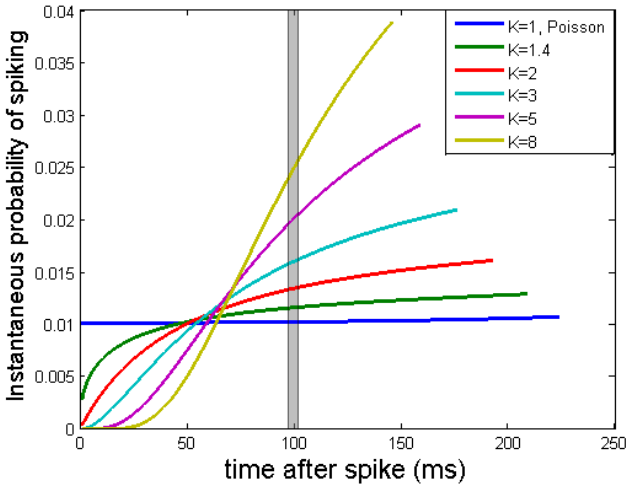


Figure 3: Recovery functions $\lambda_2$ calculated from gamma distributions of various shapes. Especially for lower shape parameters $k$, the recoveries look like long relative refractory periods.

$$\lambda_1\lambda_2(x)dx = \frac{p(x)dx}{1-\int_0^x p(t)\,dt}.$$

It remains to actually specify the form of $\lambda_2$. We define it in such a way that the mIMI model and the TRRP model are indistinguishable when firing at $c$ Hz, the average firing rate for both models. We do this in order to match the regularity properties of the mIMI with those of the TRRP as closely as possible. Our objective is to show that even though the mIMI can be as highly regular as a TRRP, it lacks the higher $\mathbf{SS} = \dfrac{1}{\mathbf{CV}}$ attained by the latter. Instead, $\mathbf{SS} = 1$ for the mIMI model matched in this manner to the TRRP and we conjecture that $\mathbf{SS} = 1$ for the mIMI model irrespective of the form of $\lambda_2$. However, we were not able to prove this result and will instead only show that it holds for a diversity of $\lambda_2$s, in particular for those obtained from TRRPs with gamma distributions. Here is the expression for $\lambda_2$ matched to a gamma distribution at $c$ Hz:

$$\lambda_2(x) = \frac{1}{c}\frac{f(x;k,\frac{1}{ck})}{1-\int_0^x f(t;k,\frac{1}{ck})\,dt},$$

where $f(x;k,\theta)$ is the notation for the probability density of the gamma distribution ((2.1)). We show what $\lambda_2$ looks like for different gamma distributions in figure 3. Once we obtained $\lambda_2$ computationally we determined ISI distributions for mIMI processes at different inputs $x = \lambda_1$ by using (4.11). These distributions helped us identify both the mean $\dfrac{1}{\langle \mathrm{ISI}\rangle}$ and the variance $\dfrac{\mathbf{CV}^2}{\langle \mathrm{ISI}\rangle}$ of the spike counts. The mean defines an input-output function $Y(x) = \langle N\rangle$, where $\langle N\rangle$ is the average number of spikes. For large enough windows the distribution of spike counts around the mean is approximately gaussian so we can apply the same argument as for the TRRP to show that the maximum likelihood decoder is just

$$G(n) = Y^{-1}(n). \tag{4.12}$$

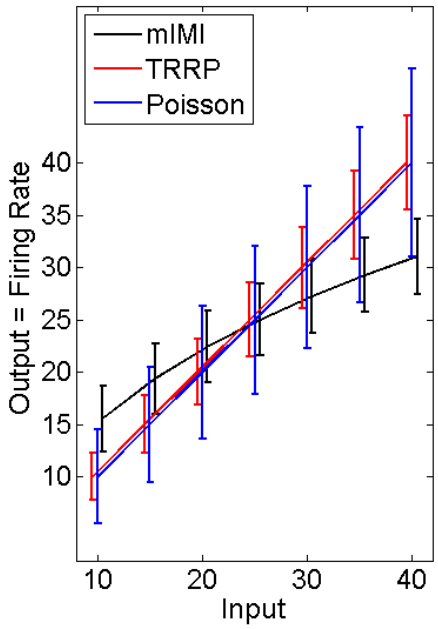


Figure 4: The three models we investigated respond differently to the same input. The error bars are standard deviations of the firing rates in 500 ms. The mIMI and TRRP models are matched to have the same distribution of ISIs - $\Gamma\left(4, \frac{1}{4c}\right)$ in response to the mean input $c = 25$. Notice the TRRP and Poisson have the same input-output function but the TRRP is less variable. Also, the TRRP and mIMI are as variable but the latter has a less steep input-output function, with a slope of about half that of the TRRP.

Importantly, in all cases we have simulated (various matching TRRP distributions among which gamma TRRPs with various shape parameters and various mean firing rates $c$) we found $Y$ to be approximately linear. We plan in future work to develop a more substantial argument than this but for now we use our observation as an approximation. We conjecture that

$$Y(x) \approx cT + A\,cT(x - c), \tag{4.13}$$

where $A$ is some parameter that needs to be estimated from simulations. We illustrate the observation in figure 4. We used in equation (4.13) the fact that $Y(c) = cT$ because we have defined it to match the firing rate of the TRRP model at $c$ Hz. As another intriguing but crucial observation, we noticed that $A \approx \mathbf{CV}(c)$ for all mIMI processes that we simulated (see figure 4). $\mathbf{CV}(c)$ should be understood as the $\mathbf{CV}$ of the distribution of ISIs when the model is firing at $c$ Hz. It follows from equations (4.13) and (4.12) that

$$G(n) = \frac{n - cT}{A\,cT} + c,$$

which we use to get the expected squared error from equation (4.4)

$$
\begin{aligned}
\mathrm{E}(err^2) &= \int_0^\infty \sum_{n=0}^{\infty} \left[ \frac{n - cT}{A\, cT} + c - x \right]^2 F(x,n)\, dp_I(x) \\
&= \frac{1}{A^2T^2c^2} \int_0^\infty \sum_{n=0}^{\infty} [n - cT - AcT(x-c)]^2\, F(x,n)\, dp_I(x) \\
&= \frac{1}{A^2T^2c^2} \int_0^\infty \mathrm{Var}(\eta_x)\, dp_I(x) \\
&= \frac{1}{A^2T^2c^2} \int_0^\infty \mathbf{F}(T)\mathrm{E}(\eta_x)\, dp_I(x) \\
&\approx \frac{1}{A^2T^2c^2} \int_0^\infty \mathbf{CV}(\mathrm{E}(\eta_x))^2 \mathrm{E}(\eta_x)\, dp_I(x) \\
&\approx \frac{\mathbf{CV}(\mathrm{E}(\eta_x))^2}{A^2Tc} \\
&\approx \frac{1}{Tc}.
\end{aligned}
$$

We approximated the expression above three times to get $\mathrm{E}(err^2) \approx \frac{1}{Tc}$. Our approximations are motivated by the observation that $A \approx \mathbf{CV}(c)$ and by the observation that $\int_0^\infty \mathbf{CV}(\mathrm{E}(\eta_x))^2\, p_I\left(\frac{x}{cT}\right)\, dx \approx \mathbf{CV}(c)^2$ which holds if the range of $\mathbf{CV}$'s is relatively small. We also used $\mathbf{F}(T) \approx \mathbf{CV}(\mathrm{E}(\eta_x))^2$ if $T$ is large enough. Plugging the expected error into equation (4.5) we get $\mathbf{SS} = 1$ for mIMI processes, irrespective of their regularity ($\mathbf{CV}(c)$). The clearest way to understand this result is to note that the slope of the input to output function (from $x$ to spike counts) of mIMI neurons is smaller than for TRRPs which have the slope 1. We believe a deeper reason must exist for having $\mathbf{SS} \approx 1$ for mIMI models but we do not understand it yet. A similar apparent equivalence was found by Prescott & Sejnowski (2008) as we showed in section 4.1, although the authors of that study interpreted it differently.

Intuitively, $\lambda_2$ contains no information about $\lambda_1$ for the mIMI process. But writing TRRPs in the same form as we wrote mIMIs in equation (4.10), we have

$$
\lambda(t) = \lambda_1(t) \cdot \lambda_2 \left[ \lambda_1 \cdot (t - s_*(t)) \right],
$$

(To see why this works see the TRRP's defining equations (3.1) and (3.2)). We therefore see that $\lambda_2$ actually does contain information about $\lambda_1$ in this case. There is probably a long way from these intuitions to the claim that mIMI processes contain as much information (per spike) as Poisson processes.

# Part II

# Neurons in a rat motor area (FOF) are time-rescaled renewal processes

## 5 Gamma shape estimator for non-stationary processes

### 5.1 Introduction

Like $\mathbf{CV_2}$, the gamma shape estimator $\mathbf{K}$ is obtained from the associated sequence $CV_2(n) = \frac{2|\mathrm{ISI}_{2n} - \mathrm{ISI}_{2n-1}|}{\mathrm{ISI}_{2n} + \mathrm{ISI}_{2n-1}}$ [5]. We define

$$\mathbf{K} = \frac{2}{\langle CV_2^2 \rangle} - \frac{1}{2}.$$

Intuitively, this is a regularity measure for the same reason $\mathbf{CV_2}$ is. If we write $\eta(n) = \frac{\mathrm{ISI}_{2n}}{\mathrm{ISI}_{2n} + \mathrm{ISI}_{2n-1}}$ then $CV_2(n) = 4\left|\eta(n) - \frac{1}{2}\right|$ and if we take into account that $\mathrm{E}(\eta) = \frac{1}{2}$ we see that both $\mathbf{CV_2} = \langle CV_2 \rangle$ and $\langle CV_2^2 \rangle$ are measures of the width of the distribution of $\eta(n)$. In fact, $\langle CV_2^2 \rangle$ is an estimate of the variance of $\eta$. A tighter distribution of $\eta$s will be obtained if the ISIs have similar values, which is to say, if the ISIs come from a tighter distribution. Because the $\eta$s are ratios, ISIs are normalized and therefore they contain no information about the intensity of the process.

The motivation for using $\mathbf{K}$ instead of $\mathbf{CV_2}$ comes from the derivation in the following section which shows that for gamma distributions $\mathbf{K}$ is precisely the shape parameter. $\mathbf{CV_2}$ on the other hand is consistently higher than $\mathbf{CV}$ for gamma processes with shape parameters $> 1$. Also, the measure $Lv$ of Shinomoto et al. (2003) is obtained in a very similar way but they define $Lv$ to be

$$Lv = \frac{3}{4}\langle CV_2^2 \rangle.$$

They claim that $Lv$ is an approximation of $\mathbf{CV}$ or that it otherwise constitutes a good new measure of local variability. We think $\mathbf{K}$ is a more intuitive measure to define, because it connects to the shape parameter of gamma distributions, which we know to fit spiking data well. If an estimate of $\mathbf{CV}$ is required one has only to make the approximation $\mathbf{CV} \approx \frac{1}{\sqrt{k}}$ which holds precisely for gamma processes.

[5] for an explanation of why we do not use any two consecutive ISIs like Holt et al. (1996) and Compte et al. (2003) see section 5.3 on error bars below

## 5.2 Derivation for gamma processes

We first determine the distribution of $\eta$. We view two consecutive ISIs as the outcomes of two iid random variables $\alpha, \beta$ each with the same gamma distribution. To determine the distribution of $\eta = \dfrac{\alpha}{\alpha+\beta}$ we set conditions $x < \dfrac{a}{a+b} < x+dx$ for $x \in [0,1)$ and determine the size of this set under the measure $d\alpha \cdot d\beta$. The conditions are equivalent to

$$\frac{a}{x+dx} - a < b < \frac{a}{x} - a.$$

If $q$ is the density of $\eta = \dfrac{\alpha}{\alpha+\beta}$ and $p$ the density of $\alpha$ and $\beta$ we have

$$\begin{aligned} q(x)dx &= P\left\{x < \frac{a}{a+b} < x+dx\right\} \\ &= \int_0^\infty \left( \int_{\frac{a}{x+dx}-a}^{\frac{a}{x}-a} p(b)db \right) \, p(a)da. \end{aligned}$$

In the limit of small $dx$, we can approximate the inner integral with $\dfrac{a}{x^2} p\left(\dfrac{a}{x} - a\right) dx$ and simplify $dx$ to get

$$q(x) \cdot x^2 = \int_0^\infty ap\left(\frac{a}{x} - a\right) p(a)\, da$$

Next we substitute $p(x) = x^{k-1} \dfrac{e^{-x/\theta}}{\theta^k \Gamma(k)}$ and the integral becomes

$$\begin{aligned} q(x)x^2 &= \frac{1}{\theta^{2k}\Gamma(k)^2} \int_0^\infty a \; a^{k-1} \left(\frac{1-x}{x}\right)^{k-1} e^{-\left(\frac{a}{x}-a\right)/\theta} a^{k-1} e^{-a/\theta} \, da \\ &= \frac{1}{\theta^{2k}\Gamma(k)^2} \left(\frac{1-x}{x}\right)^{k-1} \int_0^\infty a^{2k-1} e^{-a/(x\theta)} \, da \\ &= \frac{1}{\theta^{2k}\Gamma(k)^2} \left(\frac{1-x}{x}\right)^{k-1} (x\theta)^{2k} \, \Gamma(2k) \\ &= (1-x)^{k-1} \, x^{k+1} \frac{\Gamma(2k)}{\Gamma(k)^2}. \end{aligned}$$

In the calculation of the integral above we used the fact that $a^{2k-1} \dfrac{e^{-a/(x\theta)}}{(x\theta)^{2k}\Gamma(2k)}$ is just the density of a gamma distribution with shape parameter $2k$ and scale parameter $x\theta$ and it therefore integrates to 1. We are left with a simple polynomial distribution

$$q(x) = \begin{cases} \frac{\Gamma(2k)}{\Gamma(k)^2} \left[x(1-x)\right]^{k-1} & \text{if } 0 \le x \le 1; \\ 0 & \text{otherwise.} \end{cases} \tag{5.1}$$

Notice equation 5.1 implies that $\int_0^1 \frac{\Gamma(2k)}{\Gamma(k)^2}\,[x(1-x)]^{k-1}\,dx = 1$ because densities have to integrate to 1. We will use this property in conjunction with $\mathrm{E}(\eta) = \frac{1}{2}$ and integration by parts to compute the variance of $\eta$, which we do next.

$$\begin{aligned}
-2\mathrm{Var}(\eta) &= 2\left((\mathrm{E}\eta)^2 - \mathrm{E}\eta^2\right) \\
&= \mathrm{E}\eta - 2\mathrm{E}\eta^2 \\
&= \frac{\Gamma(2k)}{\Gamma(k)^2}\int_0^1 x(1-2x)[x(1-x)]^{k-1} \\
&= \frac{\Gamma(2k)}{\Gamma(k)^2}\left(x\frac{[x(1-x)]^k}{k}|_0^1 - \int_0^1 \frac{[x(1-x)]^k}{k}\,dx\right) \\
&= -\frac{\Gamma(2k)}{\Gamma(k)^2}\frac{\Gamma(k+1)^2}{\Gamma(2k+2)}\frac{1}{k} \\
&= -\frac{1}{2(2k+1)}.
\end{aligned}$$

We used the functional equation of the gamma function $\Gamma(t+1) = t\Gamma(t)$. It follows from here that $k = \frac{1}{8\mathrm{Var}(\eta)} - \frac{1}{2}$ or $k \approx \mathbf{K} = \frac{1}{\langle CV_2^2\rangle} - \frac{1}{2}$ if we observe that $\langle CV_2^2\rangle = 16\langle(\eta(n) - \frac{1}{2})^2\rangle$. Thus we have obtained an indirect method for estimating the shape parameter of processes that are given by non-stationary gamma distributions. We validated the formula by performing computational simulations of gamma processes and in all cases the formula returned values very close to the actual shape parameter used in the simulation.

### 5.3 Error bars

In order to tell how good of an approximation the formula gives with finite data, we compute error bars on $\mathbf{K}$ by bootstrapping the available samples 10000 times. If the distribution of the bootstrapped values is close to Gaussian, then the actual shape parameter $K$ is with 67% probability within one error bar from the computed $\mathbf{K}$ and with 95% probability within two error bars (Davison & Hinkley (1997)).

We verified that the bootstraps are normally distributed by fitting a Gaussian to each distribution. First we determined the mean $\mu$ and standard deviation $\sigma$ of the maximum likelihood Gaussian that fits the empirical distribution, then we binned the empirical distribution in 60 bins of size $\sigma/10$ each around the mean $\mu$. Then we calculated the R-square of the fit with the Gaussian $\mathcal{N}(\mu, \sigma)$ to the binned empirical distribution. For the rat data, the R-square of the fits was on average 0.91 $\pm$ 0.0051 (mean $\pm$ sd) across the population of 266 neurons analyzed. This shows that the distributions of the bootstraps are close to normal. To speed up data processing, we will in this work make judgements about the probabilities of certain events based only on the error bars. For example, if we have two

sets of $CV_2$s from which we want to compute **K**s we will consider the two values of **K** significantly different at the 5% probability level if the error bars do not overlap.

Notice that the derivation in the previous section assumes that every instance of $\eta(n) = \dfrac{\mathrm{ISI}_{2n}}{\mathrm{ISI}_{2n} + \mathrm{ISI}_{2n-1}}$ is independent from every other instance. This is the reason we do not use all possible pairs of consecutive intervals like Holt et al. (1996) do in the derivation of $\mathbf{CV_2}$. While **K** should still converge to $k$ when we use all possible pairs of consecutive ISIs, the bootstrapping procedure would be affected and the error bars would no longer be reliable because observations are not independent.

### 5.4 Spike trains are well approximated by gamma processes

Unfortunately we are unable to directly fit distributions of ISIs to show that the neurons in our data are gamma processes because we do not have well aligned trials from which to compute the PSTH and estimate intensities like Softky & Koch (1993) and Maimon & Assad (2009). The rats from which the data comes responded freely and the neurons in FOF showed very little response to the stimuli. We do however note that spike trains from other datasets (Maimon & Assad (2009)) have been shown to be well approximated by gamma processes.

We can also offer some indirect evidence that the neurons in the rat dataset are gamma processes. Since we can readily obtain empirical distributions of $\eta$, we can fit these distributions with polynomials of the form $\dfrac{\Gamma(2k)}{\Gamma(k)^2}\left[x(1-x)\right]^{k-1}$ and look at the goodness of the fits. For the rat data the mean R-squares were $0.87 \pm 0.067$ with a median of 0.88. Figure 5(a) shows fits to actual data obtained from rat neurons.

The tightness of the distribution of R-squares suggests that the R-squares are near their maximum possible values. That limit is set by the inherent stochasticity in the data, which occurs because a finite number of pairs of ISIs (2000 to be precise) were used to generate each distribution. To get more power, we pooled together distributions of $\eta$ of similar variances from different neurons and even different animals and did the fits again. Notice we are NOT pooling together distributions that look like the polynomial distributions we want to fit. If that was the case of course we would end up with better fits but it would prove nothing. We are just selecting neurons based on the variances of their distributions. The average R-squares went up to 0.9832. Figure 5(b) shows 6 examples for different variances of $\eta$. We only saw a significant difference from the model for $K \leq 1.4$. In fact, if we exclude $K \leq 1.4$, average R-square fits were 0.9954 on average. The very few cells which contributed data to values of $K \leq 1.4$ seemed to be slightly bursty. Notice in figure 5(b) for $k = 1.2$ the probability is highest near 0 and 1, which is an indicator of either bursty cells or cells with distributions very skewed towards infinity. $\eta(n) = \dfrac{\mathrm{ISI}_{2n}}{\mathrm{ISI}_{2n} + \mathrm{ISI}_{2n-1}}$ can only be close to 0 or 1 if one of $\mathrm{ISI}_{2n}$ and $\mathrm{ISI}_{2n-1}$ is either very small or very large.

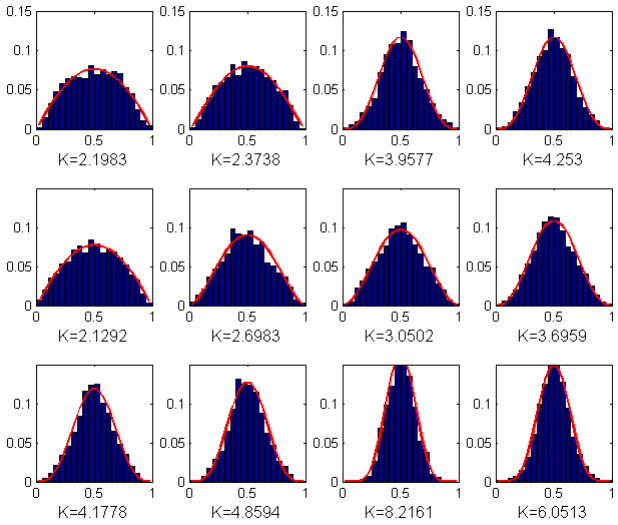


(a)

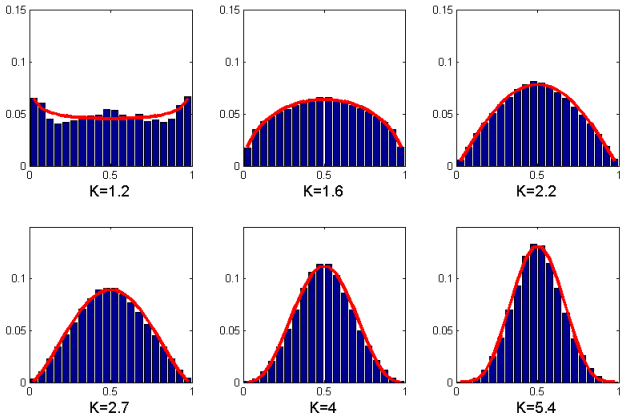


(b)

Figure 5: **a.** An empirical distribution of the random variable $\eta$ was obtained from actual spiking data. 2000 pairs of ISI's were used to generate each distribution. Polynomials of the form $\frac{\Gamma(2k)}{\Gamma(k)^2}\left[x(1-x)\right]^{k-1}$ were fitted to these distributions to obtain the best fit $k$. 12 example fits are shown for different cells and various $k$s. These overall good fits (average R-square 0.87) are indirect proof that the distributions of ISIs are actually gamma. **b.** We further pooled together pairs of ISIs from cells that had similar variances of $\eta$. The new R-square fits were 0.9954 on average.

If in addition we would have been able to prove that the transformation which takes a random process and generates $\eta$ is one to one and reasonably well-behaved, we would have been able to show directly that the spike trains are gamma processes. However, since we were unable to prove this, high values of R-squares are only indirect evidence that the spike trains are gamma processes. Notice though that even if the spike trains are not gamma processes, $\mathbf{K}$ is still a sensible measure of their regularity.

In addition, notice in figure 5(a) that the high regularity effects cannot be explained by absolute refractory periods. A Poisson process with an absolute refractory period is expected to generate a distribution of $\eta$ that is mostly flat except at the extreme ends where it falls dramatically to 0, which is not the case in our data (see the equivalent distributions of $\mathbf{CV_2}$ in Compte et al. (2003)). In section 4.5 we showed that gamma processes with low $\mathbf{k}$s (see figure 3) can be interpreted as spike trains with long relative refractory-like periods.

# 6 Data analysis I - monkey PFC data

We start illustrating our methods for calculating gamma shapes on the PFC data set. However, the results we obtain here do not directly contribute to the main thesis of this paper, that regular TRRPs are more efficient rate coders and that we should be able to observe them in systems where a rate code is used. Instead, this entire section should be seen as a digression from that topic and the results we report here should be considered separately from the rest of the paper.

## 6.1 The task

The first of the two data sets we analyzed comes from macaque monkeys. The task is described in detail in Romo et al. (1999) and Brody et al. (2003). We briefly describe the task here, focusing on those details that will be needed to understand the analysis of the statistical properties of the spike trains.

A trial was initiated when the monkey pressed a lever. The first stimulus (ST1) was presented to the monkey after a random wait period of at least 1500ms. ST1 was a vibrotactile stimulus applied to a finger of the monkey at a certain frequency $f_1$ for 500ms. After a delay period of 3000ms a second stimulus (ST2) was presented, which was like ST1 a vibrotactile stimulation but at a different frequency $f_2$ for another 500ms. The monkey was required to compare $f_1$ and $f_2$ and press one of two levers to indicate which stimulus had a higher frequency. Electrophysiological recordings in the prefrontal cortex revealed a set of neurons with responses correlated with the first stimulus $f_1$ during the delay period, making these neurons candidates for the neural substrate of the short-term memory of $f_1$. However, only a subset of these had persistent $f_1$-dependent responses throughout the 3 seconds long delay period. Most units had such responses only at certain times during the

delay period. There were also recordings from areas S2 and M1, during performance of the same task, but most of the cells recorded there did not show significant memory-related activity.

Each neuron was recorded on average with 100 trials. We analyzed neural responses starting at -2000ms from the onset of the first stimulus to 1000ms after the offset of the second stimulus, for a total of 7 s per trial and a grand total of 700s of recorded activity per neuron, on average. Firing rates in PFC averaged between 10 and 15 Hz, so for most of the neurons recorded we had between 7000 and 10000 ISI's available for our statistical analysis.

### 6.2 Gamma shape K analysis

For the analysis of the gamma shape we first binned the data for each neuron. We chose 500ms as the size of the bin. The first stimulus period was one of the time bins (the fifth) and the second stimulus period was another (the 12th). The PFC dataset consisted of 992 neurons but some of these might have been multiunits. The mean of $\mathbf{K}$ during fixation (first 4 time bins) and delay (time bins 6-11) was $1.43 \pm 0.75$ (mean $\pm$ SD, SEM$=\frac{\text{SD}}{\sqrt{n}} = 0.024$), significantly different from 1 (Poisson) but not from each other. The full distribution of $\mathbf{K}$ values is shown in figure 6(c).

Note that Compte et al. (2003) analyzes a similar dataset, also from dorsolateral PFC and also during a short-term memory task, but they do not find their units to be significantly different from what the Poisson model predicts. One reason could be that $\mathbf{CV_2}$ intrinsically makes the data more Poisson-like, by overestimating the coefficient of variation below 1 and underestimating it above 1, but the more serious flaw in their analysis is to use standard deviation rather than standard error of the mean for establishing significance. We suspect that their data is, like the data presented here, significantly different from the Poisson model.

The second difference from the data analyzed in Compte et al. (2003) is that the same neurons have significantly different statistics during fixation than during delay (we base this observation on visual inspection of the distributions in figure 2b of their paper). In fact, by drawing a parallel with our data, we believe this effect to be larger than any of the effects we report here in PFC.

Continuing with the analysis, mean $\mathbf{K}$ increased significantly to 1.58 and 1.68 respectively during the two stimulus periods, but there was also a significant increase in firing rate, which almost doubled from $\sim$12 Hz to $\sim$23 Hz. This correlation could be explained by the constancy of absolute and/or relative refractory periods, as firing rates increase.

Next we sought differences between the statistics of neurons that were actually holding the memory and the statistics of neurons that were not. To that end, we divided the data

into three sets: the top 5% memory encoders, the next 25% memory encoders and the rest of the units. We judged goodness of encoding with methods similar to those of Romo et al. (1999). For each of the 6 time bins that made up the delay period, we regressed the firing rates of each neuron to the value of $f_1$. The regression returns a p-value which we used as an indicator of the goodness of memory encoding for that time bin. To get a global measure we simply added the 6 p-values obtained in each time bin. For the top 5% memory encoders (50/992), the sum of the 6 p-values was less than 0.1 and for the next 25% (240/992) the sum was less than 1.5. The resulting mean **K** values for each time bin for each of the three sets is shown in figure 6(a). Clearly, the better and best memory encoders tend to be described by increasingly more regular processes.

Like before, this effect could have simply been a consequence of the refractory period at higher firing rates, so we also present the data in a firing rate - **K** plot in figure 6(b). The data points on that plot represent the same information as that in figure 6(a). Both effects can be observed on this plot: 1) higher firing rate correlates with higher **K** for the same set of neurons but also, 2) for different sets of neurons firing at similar rates there are significant differences among **K**'s. We conclude that good memory encoders have higher **K** by virtue of both a higher average firing rate and a higher intrinsic regularity.

We also analyzed data from brain areas S2 (703 units) and M1 (322 units) recorded during performance of the same task. Units in these areas show task-dependent responses Brody et al. (2003). Average **K** values for the S2 units was 1.26±0.74 (sem=0.028) while for the M1 units, average **K** value was 1.41±0.98 (sem=0.055). Average firing rates in S2 and M1 were very similar to those in PFC.

### 6.3 Fano Factors

Next we determined the Fano Factor for the same units recorded in PFC. Recall that the Fano Factor will be a function of both within trial statistics of the spike trains and also of across trial variations between spike trains. For example, if the spike trains were perfect Poisson processes of the exact same intensity in every trial, then the Fano Factor would be exactly 1. However, if there was also variation in the intensity of the process for different trials, then the Fano Factor will be expected to be larger than 1.

For this analysis we computed average firing rates and variances for 100ms, 200ms and 400ms time bins separately, for the same time range for which we calculated **K**. We averaged the individual Fano Factors within the same three sets of units: top 5% memory encoders, next 25% memory encoders and the rest. Figure 7 shows the time courses of average Fano Factors of the three sets of units for the three bin sizes used.

Notice first that the Fano Factors are on average larger than 1 whereas in a previous section we determined that the processes are in fact more regular than the Poisson process.

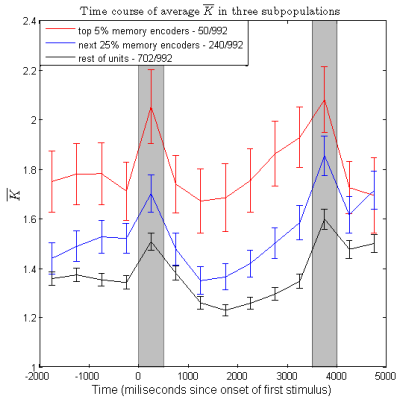


(a)

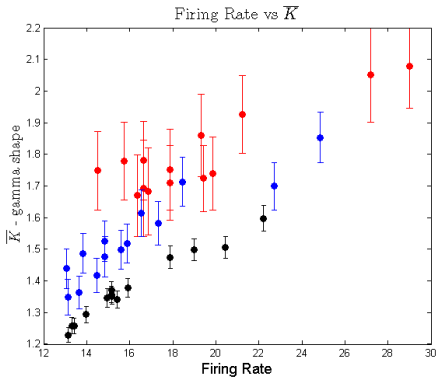


(b)

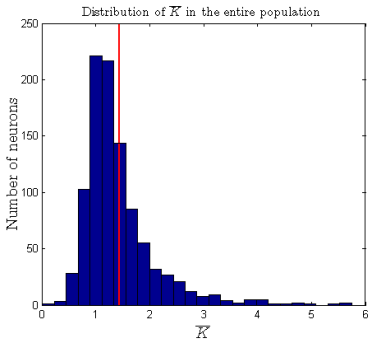


(c)

Figure 6: We divided the population of 992 units in 3 sets based on how well they encoded $f_1$. a) The time course of average **K** for each of the three sets. Error bars are standard error of the mean. The shaded areas represent the two stimulus periods. For almost all time bins, the three sets have significantly different **K** values. b) The same values of **K** are plotted versus firing rate in this plot. Notice for each of the three sets there is a tendency to have higher **K** with higher firing rate, but also that the better and best memory encoders have intrinsically higher regularity values than the rest of the units, even when firing at similar firing rates. c) Distribution of **K** in the population. The values shown have been averaged over the 14 time bins considered. The red line shows the mean of the distribution. Two outliers ($\mathbf{K} = 8.1$ and $\mathbf{K} = 8.3$) are not shown.

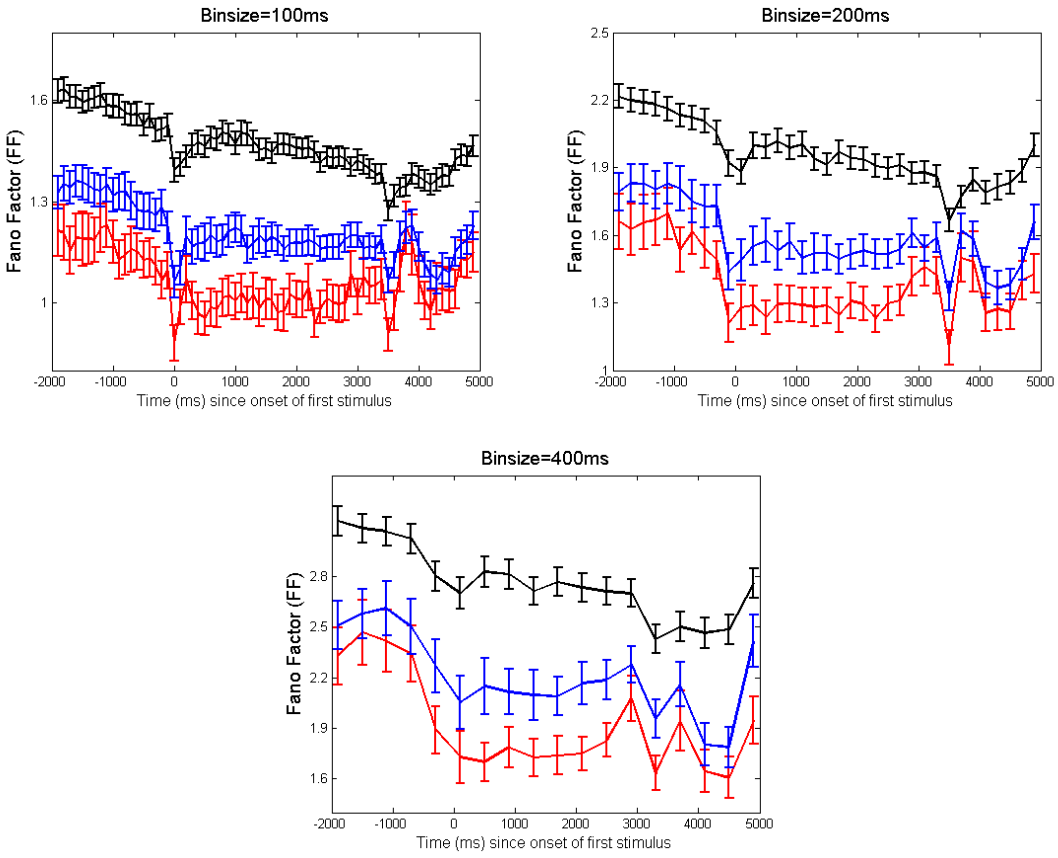


Figure 7: Fano Factors for different bin sizes and for the three different subpopulations studied. Notice that Fano Factors are greater than expected [even] from Poisson processes (1). Also, the Fano Factors seem to increase with the size of the bin used. Both effects are indicative of another source of stochasticity: the intensities of the processes vary across trials. These kinds of processes are called doubly stochastic.

The discrepancy can be explained by the additional randomness that results from variations in intensities across trials.

Notice also that for different bin sizes we obtain very different values for the Fano Factor. We believe this discrepancy is also a result of the randomness of the intensity variable.

We can see in figure 7 that good memory encoders have increased regularity, as measured by the Fano Factor.

# 7 Data analysis II - rat FOF data

## 7.1 The tasks

We did not analyze neural activity in the rats in relation with the task, but for completeness we give a brief description of the experiments that have been conducted in these animals. In one set of experiments, short-term memory and decision-making was analyzed in a delayed orienting task. Rats were required to initiate a trial by keeping their noses in a central poke for at least one second without interruption. At the end of the second, an auditory stimulus was presented from one of two small speakers on the left and on the right of the central poke. The rats were required to maintain nose poke for another 500-1000ms and only then respond by moving to the side where they heard the stimulus and respond by entering the nose poke on that side. Correct responses were rewarded with water, delivered at the correct nose poke. In a different set of experiments, the rats were presented with auditory stimuli coming from both sides of the cage. These sounds were clicks arriving at various rates with Poisson-like statistics. The rat had to determine which of the two sounds was delivered at a higher average frequency and then enter the corresponding nose poke. Neural activity was recorded with tetrodes implanted mainly in FOF, the frontal orienting fields.

## 7.2 Empirical firing rate and local regularity

The monkey PFC data which we analyzed in the previous section suggested that regularity might depend in some way on the firing rate of the process. As such, we wished to divide the set of pairs of ISIs of a neuron into subsets of pairs associated with similar firing rates. This is the approach of Maimon & Assad (2009). To do this we needed estimates of the firing rate from single spike trains.

When neural responses are highly stereotyped, such as the responses of neurons to repetitive visual stimuli (Maimon & Assad (2009)), the spike trains are well aligned to behavioral events and the firing rates may be obtained by averaging over multiple trials as Maimon & Assad (2009) did in their study of regularity. However, we did not have any good, robust marker to which to align our data, because the neurons we are analyzing are

involved in decision making / motor control.

Nonetheless, a crude estimate of the firing rate may be obtained by convolving the spike train with a relatively fat Gaussian. We chose a width of $\sigma = 250$ms. Since we do not have direct access to the actual firing rates of the spike trains, we used computational simulations to test how crude these estimates are. We simulated gamma processes with parameters in the range observed in our data, using shape parameters of $K = 1, 2, 3, 4, 5, 6$ and firing rates of Rate $= 5, 10, 15, 20, 30, 40$ Hz. For every pair of parameters we simulated 500 spike trains and determined the empirical firing rate at one time point. These 500 values were on average close to the actual firing rate used, as expected: see figure 8a. If we further look at the spread of the 500 empirical firing rates we can get an idea of how close each instance was, on average, to the actual firing rate. Figure 8b shows the standard deviation of the empirical firing rate for all parameter settings simulated.

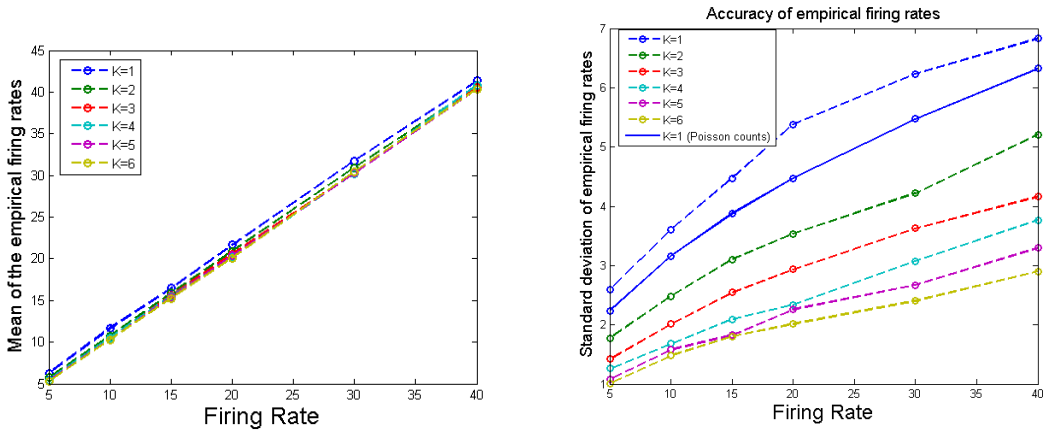


(a) Mean firing rates

(b) Standard deviations

Figure 8: We tried to obtain good estimates of firing rate from local information contained in single spike trains. For this we simulated processes of different gamma shape values and different firing rates and convolved them with a Gaussian of width $\sigma = 250$ms. The average firing rate obtained in different computational simulations closely matched the actual firing rate used. More importantly, panel (b) shows the standard deviation of the firing rates obtained. See text for more information.

Figure 8b shows two obvious effects. First, errors increase with firing rate, but actually decrease *in proportion to the firing rate*. We contend that errors of this size are acceptable for our purposes. The second effect is that the errors are smaller for higher values of the shape parameter used. This comes as no surprise, since we know that the shape parameter determines the regularity of the process. In fact, the value of $K$ sets the limit to how well we can determine the firing rate empirically from finite data. For a Poisson process, we know that the Fano Factor is 1 (Dayan & Abbott (2001)) therefore the standard deviation

of the counts in a square window of one second is equal to the square root of the firing rate. This is plotted as a solid blue line in figure 8b along with the other standard deviations and it shows that by using a Gaussian of width 250ms we are doing almost as well as we would have done by counting the spikes in a 1s window. However, using a Gaussian instead of a square filter allows us to have more temporal accuracy with real data where the firing rate is non-stationary. Using a square filter or a larger width Gaussian would be more accurate if the firing rate was stationary, but for real data we settled for a Gaussian of width 250ms. In a later section (7.5) we show how to design better kernels, custom made for each neuron, that take into account the timescale of variation of the firing rate.

We considered pairs of ISIs $\omega_n = (\mathrm{ISI}_{2n-1}, \mathrm{ISI}_{2n})$ and labeled them with the local estimate of firing rate described above. We used the labels to parse the full set of $\omega_n$s by firing rate. However, instead of considering separately $\omega_n$s obtained from $5-10$ Hz, $10-15$ Hz etc. as in Maimon & Assad (2009), we preferred to parse the $\omega_n$s into 'boxes' of size 2000 after ordering them by firing rate. As a result, we can get more resolution on the variation of $\mathbf{K}$ with firing rate. For example in some cases we got 5 boxes and in other cases we got up to 20 boxes.

### 7.3 Shape parameter K depends on firing rate

In contrast with our analysis of the monkey data, for the rat neurons we examined the dependency of regularity on firing rate. The primary reason for doing this analysis on the rat neurons is that we had many more spikes recorded from each cell, about 60000 on average, compared to 10000 on average from the monkey neurons. From 60000 spikes, 30000 independent $\omega_n$ pairs were obtained and when we further parsed them into boxes of size 2000 we got an average of 15 boxes per neuron. Recall from the previous section that each box contains $\omega_n$s coming from about the same firing rate. Since every $\omega_n$ is labeled with a local empirical firing rate, we averaged these in each box to get an approximate mean firing rate per box. Then we calculated $\mathbf{K} = \dfrac{2}{\langle CV_2^2 \rangle} - \dfrac{1}{2}$ for each box, where $CV_2(n) = \dfrac{2|\mathrm{ISI}_{2n} - \mathrm{ISI}_{2n-1}|}{\mathrm{ISI}_{2n} + \mathrm{ISI}_{2n-1}}$ (see section 5). Error bars were generated by bootstrapping.

We found that variations of $\mathbf{K}$ with firing rate were somewhat stereotyped. Several typical cells are shown in figure 9. Each row contains 4 instances of a stereotype.

The first row shows cells for which $\mathbf{K}$ increases almost linearly with firing rate across the entire spectrum of firing rates. Notice there is some variation in the slopes of the functions. In all cases $\mathbf{K}$ goes far above what a moderate (2ms) or even extreme (5-10ms) absolute refractory period would predict. If we also consider the evidence presented earlier that the spike trains are gamma processes, we conclude that the absolute refractory period is probably not a significant source of regularity.

The second row shows cells for which $\mathbf{K}$ is approximately constant across most of the

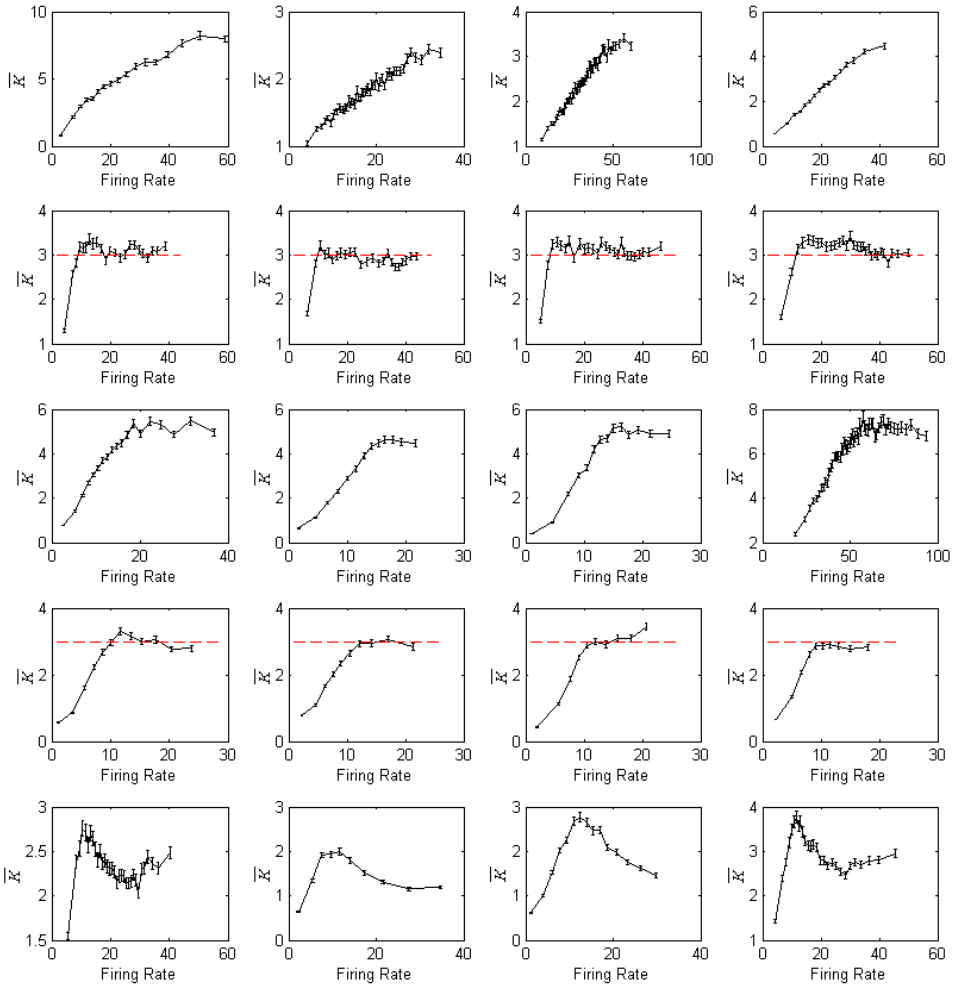


Figure 9: **K** versus firing rate plots for 16 typical cells. Each row contains cells with similar properties. See text for more information.

spectrum of firing rates. Not incidentally, the value of **K** is about 3 for all 4 cells shown. That was the case with most of the cells in this category. Notice that at very low firing rates **K** is significantly lower for all cells shown in figure 9, and in fact for all cells in our database. It is possible that this effect was an artefact of our method. If we look again at figure 8 we see that our method for determining local firing rate performs quite poorly at low firing rates. It is therefore plausible that our approximation of **K** breaks down at low firing rates.

The third row shows cells for which **K** increases with firing rate at low rates and then saturates for higher firing rates. Neurons in this class can go up to high values of **K** in the range 4-8. The fourth row shows cells with similar saturation properties, however, these cells saturate at **K** of about 3 and firing rates of about 10. These units could also belong to the class shown in the second row. If our approximation indeed breaks at low firing rates, say below 10, then it is conceivable that these units actually keep the same **K** across the spectrum of firing rates.

The fifth and last row shows cells for which we found a peak in the firing rate – **K** function.

For each cell we obtained an average value of **K** in each of the firing rate intervals $< 5$ Hz, $5 - 10$ Hz, $10 - 15$ Hz, $15 - 20$, $> 20$ Hz. We calculated the average value for each range of the firing rate ranges across cells. Notice that not every cell fired in every range of firing rates. We obtained, in order, $1.73 \pm 0.35$ (mean $\pm$ sd, n=213/266), $2.45 \pm 0.58$ (n=260/266), $3.03 \pm 0.85$ (n=262/266), $3.3 \pm 1.1$ (n=227/266) and $3.4 \pm 1.2$ (n=178/266).

### 7.4 Fano Factors

Figure 10 shows the time course of the average Fano Factor for neural data aligned to side pokes, averaged in 500ms bins. It also shows the time course of the expected Fano Factor for gamma processes with the respective gamma shapes. We can argue like we did for the monkey data and conclude that there is considerable variation in intensity across trials, aside from the variation expected from a random process. In the case of the rat neurons such variation might arise because the trials are not well aligned to relevant time markers. It is possible that these neurons respond in a stereotypical fashion but taht their responses are aligned to the animal's movements, for example.

Notice also that the Fano Factor is much smaller after time $t = 0$, that is after the rat pokes the side pokes. The main reason for this is clear. Neural data is much better aligned after a significant behavioral event than it is before the event. For example, the rat's movements might have happened anywhere in the last second before side pokes and since neural activity in FOF is correlated with movements it follows that alignment will be poor before side pokes.

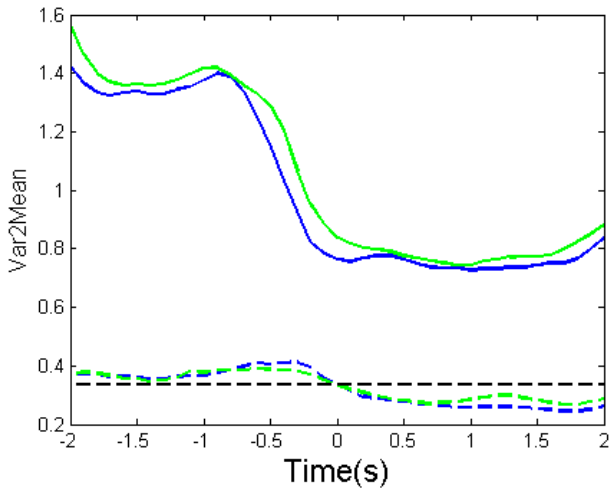


Figure 10: The Fano Factors in 500 ms windows for data aligned to the behavioral markers. At time 0 the rat poked one of two ports to receive its reward. The solid lines are the actual average Fano Factors, the interrupted lines are the expected average Fano Factors for gamma processes of the corresponding shapes. The Fano Factor for a gamma process with the mean shape parameter is shown in black. This was the only task related effect on regularity that we were able to observe.

On the same figure 10 we have drawn in black the expected Fano Factor for a gamma process of shape parameter $K = 3$, which was approximately the mean for the rat neurons. Note that the expected Fano Factor is larger than average before side poke and smaller than average after side poke. This is a different effect than that for the actual Fano Factors, and it shows that the gamma shapes are on average smaller before side poke than they are after. This was the only task-related effect on regularity that we were able to observe. We examine this effect more closely in section 7.7.

## 7.5 Designing optimal kernels

We have yet to classify neurons as candidate TRRPs or mIMIs but first we make a digression on the subject of convolution kernels. Recall that for the analysis above we used a simple gaussian kernel with a standard deviation of 250 ms. We can do better by using a nonparametric method, or in other words a method that does not assume a particular model. As a result we obtain better estimates of the local firing rate but we also obtain information about the timescale of autocorrelation of the spike train, which indirectly gives us an estimate of the timescale of autocorrelation of the input.

We fit the shape of the convolution kernel using a cubic spline basis (Hastie et al. (2001)). Formally, we write

$$\mathcal{K}_{\mathbf{a}}(t - t_{sp}) = \sum_{i=1}^{n} a_i \psi_i(t - t_{sp}), \tag{7.1}$$

where $\mathbf{a} = (a_i)$ are coefficients to be determined from the data. The $\psi_i$ are piecewise cubic functions that are linear outside of an interval. Illustrative basis elements $\psi$ are shown in figure 11(a), but for fitting $\mathcal{K}$ we used $psi_i$ with several nodes specified in advance. We

will not go into the technical details of how we constrain the basis elements to be piecewise cubic while still continuous, with continuous first and second derivatives. Suffice it to say the basis $\psi_i$ which we chose has a large capacity for fitting smooth functions.

Our objective in choosing $a_i$s is to maximize the likelihood of the observed spike train. To do this we need a model for the distribution of interspike intervals. We could just simply assume a gaussian or exponential distribution and then the fitting procedure would do fine but we can do better by using knowledge about the distribution of ISIs which we already have. We can use a gamma distribution with shape parameter $\mathbf{K}$ – the estimate we got in the previous section. To keep things simple we assumed that the gamma distribution scales with firing rate and keeps a constant shape parameter. In other words we assumed the TRRP model for the posterior distribution of intervals. We also assume that the kernel is symmetric, that is $\mathcal{K}(t) = \mathcal{K}(-t), \forall t$.

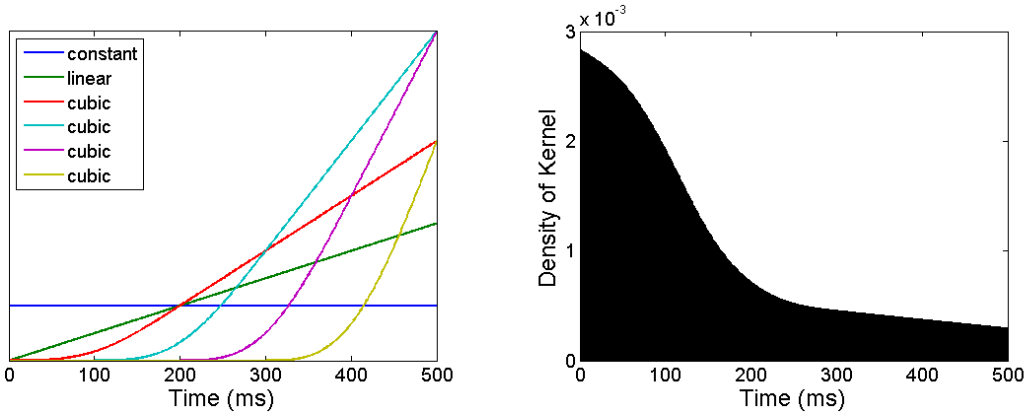


(a) A cubic splines basis

(b) One side of the average optimized kernels

Figure 11: Optimizing kernels.

We use the firing rate obtained from the convolution with the kernel to predict the ISIs in the following way. For a given kernel $\mathcal{K}$ we can compute for each ISI the local firing rate as

$$R_n(\mathbf{a}) = \int_0^{t_n} \mathcal{K}(t - t_n) \cdot \delta_t \, dt + \int_{t_{n+1}}^{\infty} \mathcal{K}(t - t_{n+1}) \cdot \delta_t \, dt, \tag{7.2}$$

where $t_n, t_{n+1}$ are the times of the $n$–th and $n+1$–th spike. Notice we avoided any information about the interval which we are trying to predict. The probability of observing $\mathrm{ISI}_n = t_{n+1} - t_n$ from a gamma distribution of intensity $R_n(\mathbf{a})$ and shape parameter $\mathbf{K}$ is simply

$$P_n(\mathbf{a})dx = f\left(\mathrm{ISI}_n; \mathbf{K}, \frac{1}{R_n(\mathbf{a})\mathbf{K}}\right) dx,$$

where $f$ is the probability density of gamma distributions (equation ((2.1))). The total probability of observing the entire spike train is then

$$P(\mathbf{a}) = \prod P_n(\mathbf{a}).$$

We use an unconstrained nonlinear optimization algorithm to maximize $P$ as a function of $\mathbf{a}$. One such algorithm available in Matlab uses the Nelder-Mead Simplex method (Lagarias et al. (1998)) and is implemented in the function *fminsearch*. Finally after we optimize $\mathbf{a}$ we can reconstruct the optimized kernels from equation ((7.1)). We are not guaranteed the best global kernel because the algorithm could in principle converge to a local minimum. In practice however we found the resulting kernels to be reasonably well-behaved, and consistent across cells.

We can draw a few conclusions from this. First, an implicit assumption for most of this work was that the input is correlated on a long timescale so that firing rates vary slowly. The kernels we obtained are evidence for this. The standard deviation of the average kernel shown in figure 11(b) is 192 ms. The fact that the kernel does not decay to 0 at long times is indicative of a correlation on an even longer timescale than 200 ms but we did not pursue this further. A second observation is that the shape of the kernel depends little on the particular cell. To see this we computed correlation coefficients between the kernels from every two pairs of cells. The average coefficient of correlation was 0.895, indicative of high similarity between all optimized kernels. Such custom designed kernels could also be of interest for obtaining firing rate estimators for brain machine interfaces (Cunninghama et al. (2009)). The standard kernel of choice — the Gaussian — might not give as good approximations of firing rate as our optimized kernels but to test this claim we would need to be in a paradigm where we are trying to predict the behaviors such as the time, direction and speed of the rat's movements.

Next we check to see if the optimized kernels give a reasonably good approximation of the local firing rate. In section 7.3 we associated a pair of ISIs with a certain local firing rate and then we parsed the collection of pairs by this associated local firing rate. Any further analysis of the dependence of $\mathbf{K}$ on firing rate depends on our local estimated firing rate being a good approximation of the actual firing rate. One way to test that is to see what the average ISIs associated with a range of firing rates is. Inverting the average ISI to $R = \dfrac{1}{\langle \text{ISI} \rangle}$ will give us an estimate of the *actual* average firing rate for that set of ISIs. Since in the next section we look at the ranges of firing rates 10-15, 15-20 ... 35-40 Hz we use the same ranges here. For each of the six ranges we get the *actual* average global firing rate across the population of neurons and plot it in figure 12(a) versus our local estimates. It can be seen that the average predictions come close to the *actual* firing rates. We also fit a line to the plot of each cell's individual local estimate versus *actual* firing rate and report

the distribution of the slopes in figure 12(b). The mean ± standard deviation of the slope was 0.9395 ± 0.14. We conclude that our optimized kernels specify the firing rates quite well and report properly the entire dynamic range of firing rates from 10 to 40 Hz. If the *actual* range of firing rates would have been radically smaller than that predicted by our estimates, then our conclusions about the dependence of **K** on firing rate would have been weaker.

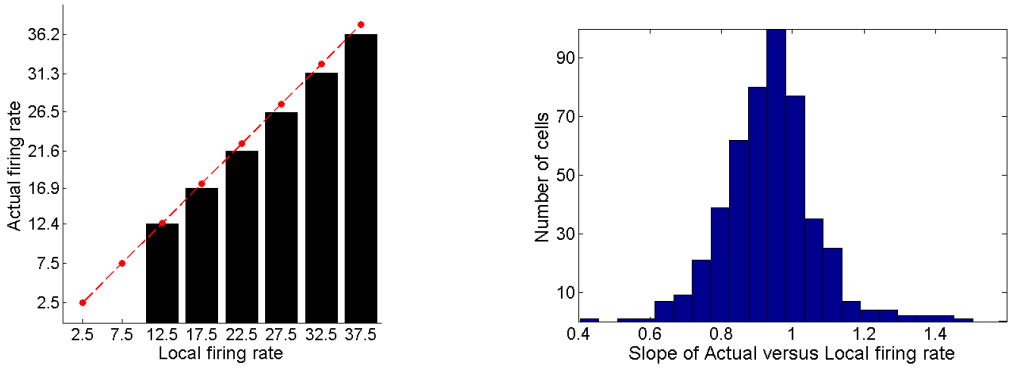


(a) (b)

Figure 12: (a) Using our optimized kernels we classified each ISI as coming from one of six ranges of firing rates. Then we calculated the $\langle ISI \rangle$ for each of the six ISI classes and compared $\frac{1}{\langle \text{ISI} \rangle}$, the *actual* firing rate, to the mean firing rate of each of the six ranges. Finally we averaged the *actual* firing rates across the entire population to get the average numbers that we plot here. The red interrupted line is the diagonal. The mean *actual* firing rates are close to our mean inferred firing rates. (b) We also fit lines to the *actual* versus inferred firing rate for each cell and we report the distribution of the slopes in this figure. The mean of the distribution is approximately 0.94.

### 7.6 TRRPs or mIMIs?

To classify neurons as TRRPs or mIMIs we defined distance metrics between the two models and the recorded cells. We divide the ISIs of each cell into the same six ranges used by Maimon & Assad (2009) from 10-15 to 35-40 Hz in increments of 5 Hz and parse the pairs $\omega_n$ of ISIs by the associated local firing rate, as calculated with the optimized kernels. We diagnosed some pairs $\omega_n$ as outliers by using the local firing rate and the gamma model and excluded them. It was necessary to do this because we would get many instances of very long ISIs ($>$ 500 ms) flanked by reasonably large local firing rates. Obviously our method for estimating the local firing rate no longer works when the ISIs become too long. Based on the gamma distribution, we excluded about 1% of the ISI pairs $\omega_n$ that would have 'rightfully' belonged to the distributions, but we diagnosed as outliers more than 5% of the $\omega_n$s on average.

We then obtain one regularity value $\mathbf{K}_i$ separately for every range of firing rates for which there are at least 300 pairs of ISIs. We did not proceed further with the analysis for cells for which we could not obtain at least 3 distinct $\mathbf{K}_i$ values. In total we were left with 504 cells from 5 rats. Notice at the time of this analysis we had more cells available than we had for section 7.3.

First we classified a proportion of the cells as significantly decreasing or peaked. These are cells of the last type shown in figure 9 and they would obviously not be fit well either by the TRRP (which predicts approximately constant shape parameters) or by the mIMI (which predicts that the shape parameter increases with firing rate). Denote by $L \in \{1, ..., 6\}$ the index of the maximal firing range available for a cell. In most cases $L$ was 6. To classify that cell as decreasing we required the following two conditions to be true

$$j = arg\,(max\,\mathbf{K}_i) < L, \text{and}$$
$$\sum_{i=j+1}^{L} \frac{\mathbf{K}_j - \mathbf{K}_i}{\mathbf{K}_j} > 0.15(L-j).$$

These conditions were chosen to match our intuitive grasp of when a neuron is significantly decreasing. 44 cells were classified as decreasing or 9% of the population.

For the remaining cells, the distance to the TRRP model is defined as

$$d_{\text{TRRP}} = \sqrt{\frac{\left(\sum_i (\mathbf{K}_i - \langle \mathbf{K} \rangle)^2\right)}{N}},$$

where $\langle \mathbf{K} \rangle$ is the mean of $\mathbf{K}_i$ and the sum is after those indices where $\mathbf{K}_i$ is available, if $N$ indices out of the 6 are available. This is just the standard (uncorrected) deviation of $\mathbf{K}_i$ and we think it is a reasonable index of how constant $\mathbf{K}$ is at different firing rates. The distance to the mIMI model is similarly defined to be

$$d_{\text{IMI}} = \sqrt{\frac{\left(\sum_i (\mathbf{K}_i - k_i)^2\right)}{N}},$$

where $k_i$ is the expected $\mathbf{K}$ value of an mIMI neuron with the same mean $\mathbf{K}$. To get $k_i$ we first match the distribution of the mIMI model at the average firing rate with a gamma distribution of shape parameter $\langle \mathbf{K} \rangle$, just like we did in section 4.5 in the first part. Continuing as in section 4.5 we obtain the recovery function $\lambda_2(t - t_{sp})$. Once we have the recovery function we can change the input $\lambda_1$ to different values so as to get the ranges of firing rates observed experimentally. We obtain in this way the regularity values $k_i$ of an mIMI neuron with recovery function $\lambda_2$ firing at 12.5, 17.5 ... 32.5 and 37.5 Hz. Remember from part I, section 4.5 that the gain of the input to output function of regular

mIMI models can become very small so it might be necessary to vary $\lambda_1$ a lot to get the mIMI neuron to fire in the required ranges.

We classify neurons as better described by the TRRP model than by the mIMI model if $d_{\text{TRRP}} < d_{\text{IMI}}$ and viceversa. We find that 329 of the remaining 460 cells or 65% of the entire population were classified as better fit by the TRRP model and 135 were better fit by the mIMI model, or 27% of the population. The average distance to the TRRP model for the 329 cells was 0.204, while the average distance to the mIMI model for the 135 was 0.208. Figure 13 shows a scatter plot of the distance to the mIMI model versus the distance to the TRRP model. As expected, the errors or distances are larger in proportion to the values of the gamma shape.

The average values of the shape parameters for the three subpopulations are shown in figure 14 with double standard errors of the mean. In the decreasing subpopulation the shape parameter is smaller at larger firing rates, while the opposite trend is followed by the mIMI subpopulation. We also plot in figure 14 the expected gamma shapes for the mIMI model neuron that would fit the averaged data for the mIMI subpopulation. Except for one point, the model is within two standard errors from the averaged data. The shape parameter **K** can be seen to be almost constant at 3.6 for the TRRP subpopulation, irrespective of firing rate.

### 7.7 A task related effect

We have insisted in this work on regularity being a characteristic of individual neurons, independent of firing rate for the TRRP neurons. In this section we present an exception. As we have already shown in figure 10, neurons seem to become more regular after the rats receive their water reward in the task, or alternatively, less regular during the time when the rats are moving towards nose pole for which they receive reward. We looked at the evolution of the mean **K** values in 500 ms windows around the time of reward separately for the three populations, TRRPs, mIMIs and the 'decreasing' cells. The results are summarized in the graphs of figure 15. Even though the mean firing rates went down from pre-reward to post-reward, the regularity values of TRRP neurons went up. The standard errors of the mean show that this effect was highly significant. The other two populations behaved roughly as expected: there was a slight tendency for **K** to decrease with time and therefore with firing rate for the mIMI population and **K** increased with time while firing rate decreased for the 'decreasing' population.

But we are most interested here in the TRRP population, especially as it comprises 65% of the cells. Figure 14 shows that in general mean **K** values stay approximately constant for firing rates between 10 and 40 Hz. Notice in the part of the task pre and post-reward mean firing rates are at the lower side of that range, so maybe **K** is only constant above 10 Hz.

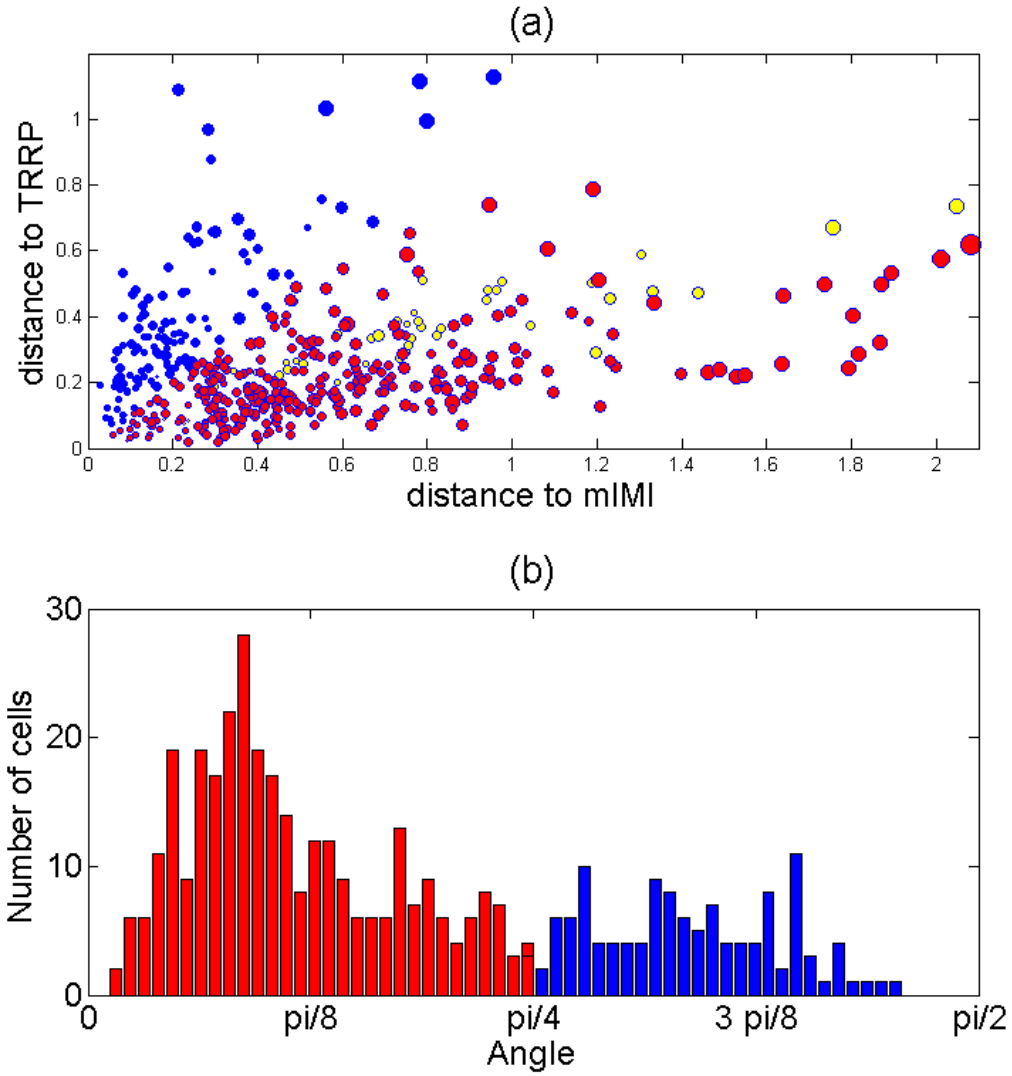


Figure 13: (a) A scatterplot of distance to the mIMI model versus distance to the TRRP model. Each filled circle represents one cell and the size of the circle is proportional to the average gamma shape **K**. Cells better described by the mIMI model are in blue while those described better by the TRRP model are in red. For completeness we also show in yellow the 9% that were classified as significantly decreasing. One blue outlier has been omitted from this figure. (b) A histogram of polar angles of red and blue circles shown in cartesian coordinates in (a); note the large peak where more TRRP units are concentrated.

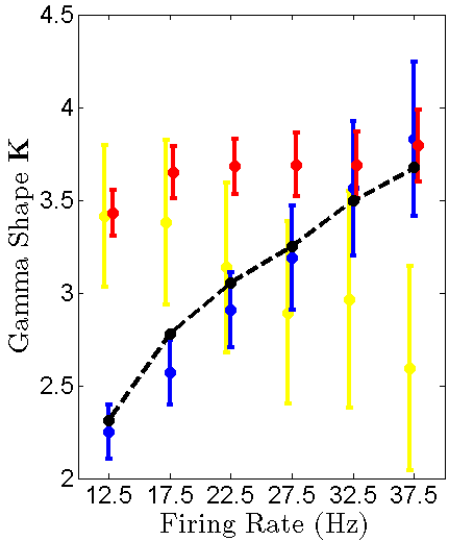


Figure 14: **K** vs firing rate for the three classes of neurons. Error bars are two times the standard errors of the mean. As before, the color code is: red = TRRP, blue = mIMI, yellow = decreasing. We fit an mIMI neuron to the mean **K** values of the blue population. The resulting fit is in black.

However, if anything we were expecting **K** to be smaller at lower firing rates, as more noise would accumulate in the intensity function of the process with longer ISIs. Instead it is larger. We cannot tell for sure here if **K** is larger than expected post-reward or smaller than expected pre-reward or both because the results in figure 14 are not completely independent from those in figure 15. All of the ISIs used to produce figure 15 had been used to produce figure 14 as well.

Also, the rats move around quite a lot and the neurons analyzed here respond strongly to movements outside the task as well, so if **K** is overall smaller during movements it would significantly affect the mean **K** values we previously got. Either way, we can say for sure that there is a difference between **K** pre-reward and **K** post-reward and we think that this might be an effect of the cumulative inputs that these neurons get from the network. Chance & Abbott (2002) showed that increasing the level of input noise in the current injected into a neuron increases **CV**. However, when there was no input and the simulated background synaptic noise was increased **CV** stayed the same. It seems therefore possible in our case that under normal conditions neurons receive balanced inputs from their local networks with varying amounts of noise but that in the pre-reward state external inputs alter this balance and increase the **CV**.

# 8 Discussion

In the first part of this work we analyzed a measure of encoding efficiency **SS** equal to the ratio between the Fisher information and the expected number of spikes and we showed that the Poisson model and the mIMI models make this measure 1 while TRRP models make the measure $\frac{1}{\mathbf{CV}}$ (see section 4.4). This shows that point processes can contain more information about the input by being more regular in the case of the TRRP model,

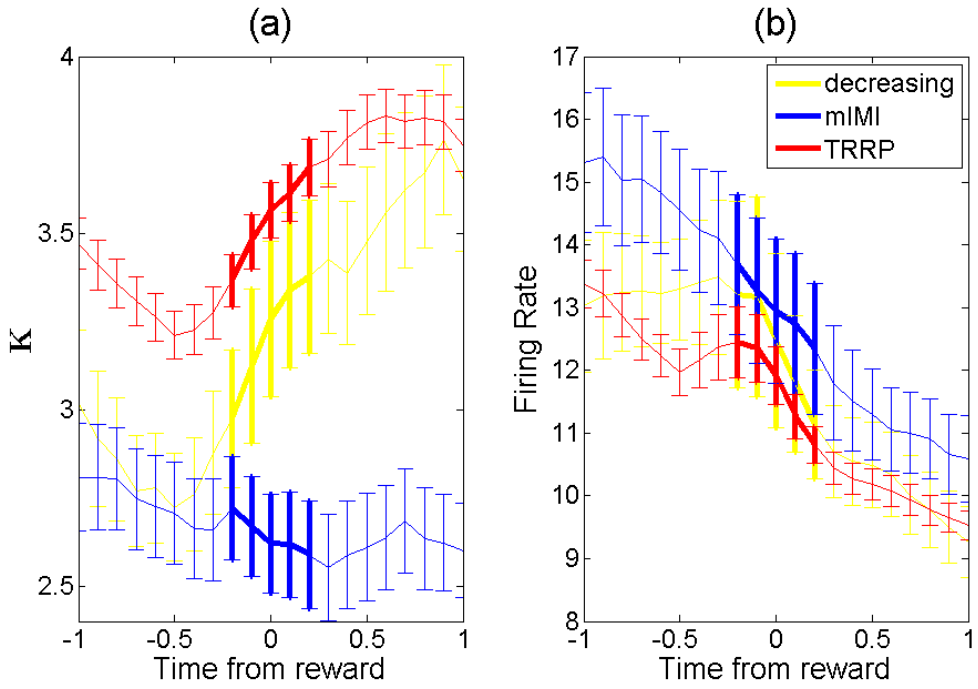


Figure 15: (a) This panel shows the evolution of the mean $\mathbf{K}$ in 500 ms windows around the time $t = 0$ corresponding to the rat entering one of two side pokes and receiving its reward. The neurons are separated into the three populations described in section 7.6. (b) Here we show the mean firing rates in the same time windows and for the same populations. Error bars are standard errors of the mean in both figures. The thicker lines represent points for which the time window overlaps with $t = 0$. All points before the thick lines are completely independent from all points after the thick lines.

but they can also not contain more information despite being more regular in the case of the mIMI model. The TRRP model achieves its efficiency by keeping the input to output function on the $x = y$ line, while for mIMI models the input to output gain has been found computationally to be $\frac{1}{\mathbf{CV}}$. Neurons from visual areas in cortex are well fitted by gamma TRRPs (Maimon & Assad (2009)) and we showed in the second part of this work that many neurons (65 %) in the dataset recorded by the Brody lab are also TRRPs. Neurons in these datasets are on **average** worth 3 Poisson or mIMI neurons in a rate code. We think we have made good progress here towards showing why neurons **should be** regular TRRPs, and not merely have a relative refractory period of fixed duration. It would not be surprising if neurons in other brain areas were found to be regular TRRPs. To start with, notice neurons in most motor areas are about as regular as those in Area 5 and FOF (Shinomoto et al. (2009)) but we do not know if they are TRRPs or mIMIs.

We also want to attract the attention of researchers to a subtlety of interpretation which we observed to be treated lightly in other publications. Softky & Koch (1993) conclude their analysis by saying that the **CV**s for neurons in V1 and MT are in the range $0.5 - 1$ and therefore the neurons fire very irregularly. However, we just showed that there is an enormous difference between $\mathbf{CV} = 0.5$ and $\mathbf{CV} = 1$ for TRRP models. A time-rescaled neuron with $\mathbf{CV} = 0.5$ has the performance of four neurons with $\mathbf{CV} = 1$ in a rate coding scheme! In fact Softky & Koch (1993) do not even report the mean **CV**s that they found. Based on visual inspection of their figure 3 and the observations in the text referring to the accuracy and biases of their method, we estimate that the average **CV**s in their analysis were about 0.7 in both V1 and MT.

An additional difficulty in interpreting **CV** is that it does not scale very intuitively. In our interpretation $\frac{1}{\mathbf{CV}^2}$ can be thought of as the number of Poisson neurons needed to achieve the same accuracy (section 4.4). Since for gamma processes $\frac{1}{\mathbf{CV}^2} = k$ we propose the gamma shape as a more intuitive correlate of regularity. The mean **CV** values observed by Softky & Koch (1993) of 0.7 approximately correspond to gamma shapes $k = 2$. These neurons would be twice as good as Poisson processes in a rate coding scheme if they were also TRRPs.

What distinguishes areas where regular neurons are found from those where regular neurons are not found? We know from the datasets of Maimon & Assad (2009), Brody and Levine & Shefner (1976) that regular TRRP neurons exist not only in different brain areas but in different systems, in different animals and even in the retina. Therefore regular neurons are not unique and probably the physical mechanisms responsible for their regularity are not unique to a very specialized set of neurons. In fact, Koyama & Kass (2008) showed that a simple leaky integrate and fire neuron can act as a TRRP, although only in the case where the signal is transmitted in the variance of the input. Also, it is a common

finding that neurons in slice with constant current injections fire very regularly and in fact the results of Chance & Abbott (2002) show that it is possible to have neurons in vitro act as regular TRRPs under simulated in vivo conditions (a large number of synaptic currents simulated by stochastic current injection, see section 3).

It therefore seems reasonable to believe that in those systems where a rate code is used, regular TRRP neurons should be expected. We can even make a stronger claim. If indeed mechanisms capable of generating regular firing are easy to employ at the single neuron level, then they MUST be employed in those systems where the rate code is used, because more efficient neurons are evolutionarily advantageous. We think that the rate code is probably employed in those systems where neurons recorded experimentally are found to fire regularly and we also think that some sort of spike timing code is employed where the neurons are found to have Poisson-like firing patterns. These two (distinct!) claims take the argument of Softky & Koch (1993) one step further. The authors of that study argue that irregular firing is inconsistent with a rate code. Shadlen & Newsome (1994) have refuted this argument by showing that an integrate and fire neuron can in fact fire irregularly. We have shown evidence that neurons **are capable of** firing more regularly and that their regular firing enhances the accuracy of the rate code because these neurons act as TRRPs. As such, the rate code should not be used in a brain system where neurons have Poisson-like statistics: it runs much more efficiently on regular TRRP neurons. Therefore a neuron with Poisson-like firing patterns must be transmitting some signal in its spike timings as well. Of course, there is always the possibility to have some combination of the two codes as well (Prescott & Sejnowski (2008)).

An especially intriguing proposal is that of Maimon & Assad (2009) that spiking in higher brain areas is more regular than lower areas. Also Shinomoto et al. (2009) show that motor areas are more regular than sensory areas. Is there a transition from a timing code to a rate code in parallel with the transition from stimulus to representation to decision to action? From an information theoretic point of view such a transition makes sense. The full capacity of the neural spike trains for transmitting information might only be necessary in sensory areas, where a lot of information is incoming from the outside world. As that information is refined and invariants of position, time, shape, form etc. are computed, the quantity of information needed to represent the environment decreases drastically. For example, to recognize a familiar face the stimulus is a huge collection of photons, say a picture of 256x256 pixels or about 200 000 bits, which is gradually transformed into contours and shapes and matched to some templates in memory. The size of the final output, the name of the familiar person for example, is at most 20 bits (assuming we can remember at most 100 000 faces and the mapping from face tokens to name tokens is less sparse than 1 to 10, a generous upper bound overall). The signal is therefore compressed at least 10 000 fold, and the compression is surely higher for objects less familiar to us

than faces. And yet, sensory areas are not 10 000 times larger in the brain than motor or executive areas; therefore sensory areas must have a much higher bandwidth per neuron than higher processing areas, consistent with sensory areas using a timing code.

But can there be an advantage in using the rate-code if it is possible to use a timing code instead? Is there a cost to the much higher bandwidth of the latter? We think yes and our explanation has to do with the robustness of computations under the two regimes. We think the rate code can guarantee far fewer errors than a timing code can. For example, many different spike trains will encode the same firing rate, but if different spike timing patterns encode different inputs then deletion or shift of a single spike can completely throw off decoders downstream. It is fine in the visual system to mistake a shade of green with another and it is fine if some contours are displaced in the processing or if some other low-level features are calculated incorrectly. However, mistaking a lion for a sheep takes miscalculation to a whole new level. Errors cannot be tolerated in high level areas. It should also be noted that the input to a neuron in a high level area is altered by all the noise that intervenes between the stimulus and that neuron. More and more noise accumulates downstream and robust encoders/decoders are desirable the further downstream one goes.

In future work we might also investigate the **SS** in cases where the distribution of the input is taken into consideration, but we think similar results should hold in those cases as well. Notice for the toy example of figure 2 that if we implement a threshold the error rate is going to be equal to one half of the area of the overlap. Since the area of the overlap is proportional to the width of the output distributions and inversely proportional to the distance between their means, it is still true that the error is a function of the input-output slope and of the regularity of the random process.

## Acknowledgements

We thank Jeffrey Erlich and Bingni Brunton for doing the rat experiments and Ranulfo Romo for doing the monkey experiments and for kindly sharing their data.

## References


Berry, M. & Meister, M. (1998), 'Refractoriness and neural precision', *J Neuro* **18**, 2200–2211.

Brody, C., Hernandez, A., Zainos, A. & Romo, R. (2003), 'Timing and neural encoding of somatosensory parametric working memory in macaque prefrontal cortex', *Cereb Cortex* **13**, 1196–1207.

Brown, E., Barbieri, R., Ventura, V., Kass, R. & Frank, L. (2001), 'The time-rescaling theorem and its application to neural spike train data analysis', *Neural Computation* **14**, 325–346.

Chance, F. & Abbott, L. (2002), 'Gain modulation from background synaptic input', *Neuron* **35**, 773–782.

Compte, A., Constantinidis, C., Tegner, J., Raghavachari, S., Chafee, M., Goldman-Rakic, P. & Wang, X. (2003), 'Temporally irregular mnemonic persistent activity in prefrontal neurons of monkeys during a delayed response task', *J Neurophysiol* **90**, 3441–3454.

Cox, D. (1967), *Renewal Theory*, Methuen.

Cunninghama, J., Gilja, V., Ryuc, S. & Shenoya, K. (2009), 'Methods for estimating neural firing rates, and their application to brain machine interfaces', *Neural Networks* **22**, 1235–1246.

Davison, A. & Hinkley, D. (1997), *Bootstrap methods and their applications*, Cambridge University Press.

Dayan, P. & Abbott, L. (2001), *Theoretical Neuroscience*, The MIT Press.

Fisher, R. (1922), 'On the mathematical foundations of theoretical statistics', *Philos Trans R Soc Lond A Phys Sci* **222**, 309–322.

Hastie, T., Tibshirani, R. & Friedman, J. (2001), *The Elements of Statistical Learning: Data mining, Inference, and Prediction*, Springer.

Holt, G., Softky, W., Koch, C. & Douglas, R. (1996), 'Comparison of discharge variability in vitro and in vivo in cat visual cortex neurons', *J Neurophysiol* **75**, 1806–1814.

Kandel, E., Schwartz, J. & Jessell, T. (2000), *Principles of Neural Science*, McGraw-Hill Medical.

Kass, R. & Ventura, V. (2001), 'A spike-train probability model', *Neural Computation* **13**, 17131720.

Kass, R., Ventura, V. & Brown, E. (2005), 'Statistical issues in the analysis of neuronal data', *J Neurophysiol* **94**, 8–25.

Koyama, S. & Kass, R. (2008), 'Spike train probability models for stimulus-driven leaky integrate-and-fire neurons', *Neural Computation* **20**, 1776–1795.

Lagarias, J., Reeds, J., Wright, M. & Wright, P. (1998), 'Convergence properties of the nelder-mead simplex method in low dimensions', *SIAM Journal of Optimization* **9(1)**, 112–147.

Levine, M. & Shefner, J. (1976), 'The effects of photic stimulation upon the variability of the interspike intervals in goldfish ganglion cells', *Vision Res* **17**, 793–797.

Machens, C., Romo, R. & Brody, C. (2005), 'Flexible control of mutual inhibition: A neural model of two-interval discrimination', *Science* **307**, 1121–1124.

Maimon, G. & Assad, J. (2009), 'Beyond poisson: Increased spike-time regularity across primate parietal cortex', *Neuron* **62**, 426–440.

Nawrot, M., Boucsein, C., Molina, V., Riehle, A., Aertsen, A. & Rotter, S. (2008), 'Measurement of variability dynamics in cortical spike trains', *J Neuro Methods* **169**, 374–390.

Prescott, S. & Sejnowski, T. (2008), 'Spike-rate coding and spike-time coding are affected oppositely by different adaptation mechanisms', *J Neuro* **28**, 13649–13661.

Ratnam, R. & Nelson, M. (2000), 'Nonrenewal statistics of electrosensory afferent spike trains: Implications for the detection of weak sensory signals', *J Neuro* **20**, 6672–6683.

Reich, D., Victor, J. & Knight, B. (1998), 'The power ratio and the interval map: Spiking models and extracellular recordings', *J Neuro* **18(23)**, 10090–10104.

Romo, R., Brody, C., Hernandez, A. & Lemus, L. (1999), 'Neuronal correlates of parametric working memory in the prefrontal cortex', *Nature* **399**, 470–473.

Sahani, M. (2007), 'The statistics of spike trains'. http://www.gatsby.ucl.ac.uk/~hehrmann/TN1/notes-spike-stats.pdf.

Seal, J., Commenges, D., Salamon, R. & Bioulac, B. (1983), 'A statistical method for the estimation of neuronal response latency and its functional interpretation', *Brain Res* **278**, 382–386.

Shadlen, M. & Newsome, W. (1994), 'Noise, neural codes and cortical organization', *Curr Op Neubio* **4**, 569–579.

Shinomoto, S., Kim, H., Shimokawa, T., Matsuno, N., Funahashi, S., Shima, K., Fujita, I., Tamura, H., Doi, T., Kawano, K., Inaba, N., Fukushima, K., Kurkin, S., Kurata, K., Taira, M., Tsutsui, K., Komatsu, H., Ogawa, T., Koida, K., Tanji, J. & Toyama, K. (2009), 'Relating neuronal firing patterns to functional differentiation of cerebral cortex', *PLOS Computational Biology* **5**, 1–10.

Shinomoto, S., Shima, K. & Tanji, J. (2003), 'Differences in spiking patterns among cortical neurons', *Neural Computation* **15**, 2823–2842.

Softky, W. & Koch, C. (1993), 'The highly irregular firing of cortical cells is inconsistent with temporal integration of random epsps', *J Neuro* **13**, 334–350.

Taneja, I. (2001), *Generalized Information Measures and Their Applications*, http. http://www.mtm.ufsc.br/ taneja/book/book.html.

vanSteveninck, R., Lewen, G., Strong, S., Koberle, R. & Bialek, W. (1997), 'Reproducibility and variability in neural spike trains', *Science* **275**, 1805–1808.